# SARS-CoV-2 Spike evolution influences GBP and IFITM sensitivity

Dejan Mesner[1], Ann-Kathrin Reuschl[1], Matthew V.X Whelan[1], Taylor Bronzovich[1] Tafhima Haider[1,2], Lucy G. Thorne[1], Greg J. Towers[1] and Clare Jolly[1]

[1]Division of Infection and Immunity, University College London, WC1E 6BT London, United Kingdom. [2]Centre for Genomics and Child Health, Blizard Institute, Queen Mary University of London, E1 2AT London, United Kingdom

Corresponding author:
Clare Jolly
c.jolly@ucl.ac.uk

Keywords: SARS-CoV-2, spike, GBP, IFITM, VOC, Omicron, restriction, innate immunity

**Abstract.**

SARS-CoV-2 spike requires proteolytic processing for viral entry. The presence of a polybasic furin-cleavage site (FCS) in spike, and evolution towards an optimised FCS by dominant variants of concern (VOCs), are linked to enhanced infectivity and transmission. Guanylate binding proteins (GBP) are interferon-inducible restriction factors that target furin-mediated processing of viral envelope proteins and limit infectivity. Here we investigated whether GBPs restrict SARS-CoV-2 infection, and whether VOCs have evolved spikes that escape restriction. We show that GBP2 and 5 interfere with cleavage of the spike proteins of Wuhan-Hu-1, Alpha, Delta and Omicron, consistent with furin inhibition by GBPs. However, while GBP2/5 restrict Wuhan-Hu-1 infectivity, Alpha and Delta escape restriction. GBP exposure in producer cells influences viral entry route into target cells, with a shift towards endosomal entry. We therefore investigated whether GBP-targeting of spike alters sensitivity to endosomal restriction factors, IFITMs. We find IFITM1, but not IFITM 2 or 3, inhibit infection of naturally-permissive epithelial cells by early-lineage SARS-CoV-2, as well as Alpha and Delta, however GBPs did not sensitise to IFITM restriction. Strikingly, we find Omicron is unique amongst VOCs, being sensitive to restriction by GBP2/5, and also IFITM1, 2 and 3. We conclude evolution of Alpha and Delta spikes have conferred resistance to GBP restriction, but this is not solely due to acquisition of an enhanced FCS. Notably, Omicron, which has evolved under different selective pressures, has selected for changes in spike that not only mediate antibody escape, and shift in cell tropism and entry, but also impact the sensitivity of Omicron to innate immunity, potentially contributing to altered pathogenesis.

## Introduction

SARS-CoV-2, the cause of the COVID-19 pandemic, infects cells by binding of the viral spike (S) protein to the angiotensin converting enzyme 2 (ACE2) receptor on host cell plasma membranes (Hoffmann et al., 2020b). Spike is a trimeric transmembrane glycoprotein consisting of an S1 ACE2 receptor-binding subunit, and the S2 subunit that drives fusion of the viral envelope with host cell membranes (Walls et al., 2020). In order for fusion to proceed after ACE2 binding, spike must be cleaved by host cell proteases to become activated and fusion-competent, thus regulating the timing and location of the viral entry process. This is step-wise process in which spike is initially processed by furin-like proteases in virus-producing cells at its S1/S2 junction (Hoffmann et al., 2020a; Walls et al., 2020). This is followed by a secondary cleavage event at the S2' site after ACE2 binding, which is mediated by the protease TMPRSS2 at the cell surface, (Hoffmann et al., 2020b), releasing the S2 domains for viral fusion at the plasma membrane. Alternatively, endocytic uptake of the virion can occur in some cell types, and in the absence of TMPRSS2, and spike can be activated for fusion by endosomal cathepsin proteases (Hoffmann et al., 2020a).

The presence of a polybasic furin cleavage site (FCS) at the S1/S2 junction of spike makes SARS-CoV-2 unique amongst sarbecoviruses (Boni et al., 2020; Temmam et al., 2022). Notably, the polybasic Arg-Arg-Ala-Arg (or RRAR) motif that is targeted by furin is absent in closely related coronaviruses, including the closest relatives of SARS-CoV-2, bat RaTG13, pangolin CoV and SARS-CoV-1 (Hoffmann et al., 2020a; Temmam et al., 2022), but is present in some other more distantly related human coronaviruses including MERS-CoV (Millet and Whittaker, 2014). This has led to the notion that evolution for a FCS in the SARS-CoV-2 ancestor was associated with successful zoonosis and pandemic transmission between humans. Indeed, this would be consistent with the ability of SARS-CoV-2 to arm itself for infection by incorporating primed or pre-processed spike into viral particles, allowing for more rapid TMPRSS2-mediated cleavage and subsequent plasma membrane fusion. In support, the FCS in SARS-CoV-2 spike has been shown to be required for efficient proteolytic cleavage of spike (Hoffmann et al., 2020a), virus infection of human airway cells (Hoffmann et al., 2020a; Hoffmann et al., 2020b; Johnson et al., 2021; Peacock et al., 2021a), cell-cell fusion and syncytia formation (Hoffmann et al., 2020a; Papa et al., 2021; Rajah et al., 2021), and transmission (Johnson et al., 2021; Peacock et al., 2021a).

Following the identification of the first SARS-CoV-2 strain circulating in humans (Wuhan-Hu-1), several variants of concern (VOCs) have emerged, each containing a constellation of mutations and further adaptations to host that have been associated with increased

transmission. These major VOCs are designated Alpha (PANGO lineage B.1.1.7), Beta (B.1.351), Gamma (P1), Delta (B.1.617.2) and latterly Omicron (B.1.1.529). Of these VOCs, Alpha, Delta and Omicron have been the most successful globally, with each VOC rapidly replacing the previous dominating VOC over time (Alpha>Delta>Omicron). A characteristic of these VOCs is the presence of an increasing number of non-synonymous mutations in spike. This includes changes in spike which alter entry efficiency and kinetics (Jackson et al., 2022) and evolution for enhanced immune escape, including innate immunity (Guo et al., 2021; Lista et al., 2021; Thorne et al., 2022). Importantly, these VOCs have evolved at different times and independently from wave-one SARS-CoV-2, not from each other, and thus were exposed to different selective pressures. For example, Alpha arose during a period where there was little population level adaptive immunity, in contrast to Omicron where significant vaccine and infection induced immunity existed. Much focus has been on spike mutations arising from selective pressure for antibody escape, however SARS-CoV-2 spike continuously adapts in other ways to the human host. This is evidenced by the dominant VOCs which harbour spike mutations near and within the FCS, suggesting potential evolution of an optimised furin cleavage site (Escalera et al., 2022; Peacock et al., 2021b). Alpha and Delta have acquired mutations at position 681 (P681H and P681R respectively). Omicron has three mutations in this region, P681H, H655Y and N679K. The optimised FCS has been reported to increase spike processing and fusogenicity for Alpha and Delta (Escalera et al., 2022; Peacock et al., 2021a; Rajah et al., 2021; Saito et al., 2022). By contrast, Omicron shows reduced fusion despite containing the same P681H mutation as Alpha (Du et al., 2022; Meng et al., 2022; Peacock et al., 2022; Willett et al., 2022). Intriguingly, Omicron, the most recent VOC, appears to also use a TMPRSS2-independent, endosomal entry pathway (Escalera et al., 2022; Meng et al., 2022; Peacock et al., 2022; Shuai et al., 2022; Willett et al., 2022). This distinguishes Omicron from preceding SARS-CoV-2 strains, including early-lineage isolates and VOCs, all of which favour TMPRSS2 usage for infection of naturally permissive human airway cells. These key differences reveal how SARS-CoV-2 can explore different evolutionary solutions by changing spike, allowing it to exploit different entry processes and modify tropism in response to various selective pressures, for example host immunity.

Successful viral replication and transmission requires evasion or antagonism of host innate immune defences, particularly for zoonotic viruses that must adapt quickly, or be suitably pre-adapted to the new host. Guanylate binding proteins (GBP) are type-1 and type-2 interferon-stimulated genes (ISGs) and a subfamily of guanosine triphosphatases (GTPases) that can act as intracellular antiviral restriction factors, with GBP2 and 5 potently interfering with furin-mediated processing of viral proteins and inhibiting infection of HIV-1,

Influenza A Virus, Zika and measles viruses for example, which all require furin cleavage for optimal infectivity (Braun et al., 2019; Hotter et al., 2017; Krapp et al., 2016; Martens and Howard, 2006). GBPs are upregulated by interferon type 1 and 2 (Martens and Howard, 2006) and during SARS-CoV-2 infection (Ziegler et al., 2020; Martin-Sancho et al., 2021). Thus, GBP proteins comprise a key effector of the antiviral innate immune response that can act to limit infectious virus production during replication. Likewise, the interferon-induced transmembrane (IFITM) protein family also acts broadly to block viral entry, inhibiting viral fusion with cellular membranes, including SARS-CoV-2 (Buchrieser et al., 2020; Lista et al., 2021; Martin-Sancho et al., 2021; Peacock et al., 2021a; Shi et al., 2021; Winstone et al., 2021). Importantly, SARS-CoV-2 sensitivity to IFITM-restriction has been shown to be influenced by mutations within the spike FCS, leading to changes in viral entry route that influences the sensitivity to IFITM2 in endosomes (Lista et al., 2021; Peacock et al., 2021a; Winstone et al., 2021). Paradoxically, in some cases IFITM2 and/or 3 can enhance SARS-CoV-2 infection by a mechanism that remains unclear (Buchrieser et al., 2020; Lista et al., 2021; Nchioua et al., 2021; Prelli Bozzo et al., 2021).

Here we investigated the capacity of GBP2 and 5 to inhibit spike cleavage and particle infectivity and tested whether evolution of spike in VOCs has led to escape from restriction. We show the differential sensitivity of SARS-CoV-2 spikes to GBPs and the effect of GBP-inhibition on spike mediated infection efficiency and IFITM restriction. We find that infection mediated by Wuhan-Hu-1 spike is sensitive to GBP restriction, but that Alpha and Delta are not. Notably, we demonstrate that the Omicron spike is similarly sensitive to GBP restriction as Wuhan-Hu-1. Strikingly, we show that Omicron is also unique amongst SARS-CoV-2 isolates in also being inhibited by IFITM2 and 3 in addition to IFTIM1, using live virus infection of Caco2 cells. In summary we conclude that evolution of SARS-CoV-2 VOCs for spike mutations has led to evasion from the spike targeting restriction factor GBP, but Omicron, is uniquely restricted by both GBP and IFITM1/2/3, consistent with Omicron displaying altered spike-mediated fusion, cell entry and tropism.

## Results

### GBP2 and 5 inhibit Wuhan-Hu-1 and Omicron, but not Alpha and Delta spike-mediated infectivity.

To establish an assay for GBP restriction, we first used HIV-1, a virus whose infectivity is potently inhibited by GBP2 and 5, blocking furin-mediated cleavage of the HIV-1 envelope glycoprotein (Braun et al., 2019; Krapp et al., 2016). As expected, exogenous expression of GBP2 and 5 in virus-producing 293T cells inhibited the infectivity of both replication-competent HIV-1, and HIV-1 Env pseudotyped virus particles (Fig. S1A-C). The

isoprenylation-deficient mutants of GBP2 (GBP2 C588A) and GBP5 (GBP5 C583A) which are mislocalised in the cell (Braun et al., 2019; Krapp et al., 2016), lost their inhibitory activity (Fig. S1B,C). To determine whether GBP 2 and 5 have activity against SARS-CoV-2 spike, which also undergoes furin-cleavage, we used a pseudovirus (PV) assay (Fig.S1A) in which SARS-CoV-2 spike is incorporated on lentiviral particles (herein termed PV). This allows direct comparison of how evolution of amino acid changes in spike alone (Fig. 1A) has influenced GBP-sensitivity, without confounding differences in other SARS-CoV-2 variant proteins on infectivity. Furthermore, infectivity can be accurately quantified by titration using the luciferase reporter gene encoded by the lentiviral backbone. 293T cells were co-transfected with plasmids encoding the variant spike and the lentiviral genome alongside increasing doses of GBP-expressing plasmid, with GBP expression confirmed by flow cytometry staining for the HA-tag (Fig. 1B, Fig. S1D). Fig. 1C shows that Wuhan-Hu-1 PV made in the presence of GBP2 or 5 was significantly less infectious (50%) when titrated onto Caco2 cells, with both GBP2 and 5 inhibiting PV infectivity in a dose dependent manner. As expected, the mutants GBP2 C588A and GBP5 C583A showed no inhibitory activity (Fig. 1C). Inhibition of Wuhan-Hu-1 PV infectivity was not due to lack of spike expression on 293T cells since expressing GBPs did not alter plasma membrane levels of spike measured by flow cytometry (Fig. S2). Notably, Alpha and Delta spikes were resistant to GBP2 and 5 restriction, with no inhibition of PV infectivity even at the highest GBP dose (Fig. 1E,F). Surprisingly, PVs containing the Omicron spike were sensitive to restriction by GBP2 and 5, behaving like Wuhan-Hu-1, showing a significant 50% loss of infectivity (Fig.1G). Consistent with the loss of Wuhan-Hu-1 PV infectivity being mediated by inhibition of furin by GBP2/5 (and not off target effects), no difference in infectivity was seen when PV were titrated onto Vero.E6 cells (Fig. S1E) that do not require furin-processing for SARS-CoV-2 infection (Hoffmann et al., 2020a; Johnson et al., 2021). Moreover, GBP2/5 expression significantly reduced infectivity mediated by MERS-CoV spike which contains a furin-cleavage site, but not by SARS-CoV-1 spike that lacks a furin-cleavage site (Fig. S1F-I).

Alpha, Delta and Omicron all contain the infectivity-enhancing D614G mutation in spike (Fig. 1A) that manifested as an early host adaptation in Wuhan-like isolates and is now ubiquitous in circulating SARS-CoV-2 variants (Korber et al., 2020; Plante et al., 2021; Yurkovetskiy et al., 2020). Interestingly, introducing the D614G mutation into Wuhan-Hu-1 spike (Wuhan-Hu-1 D614G) completely rescued PV infectivity from inhibition by GBPs (Fig. 1D). Furthermore, D614G not only rendered Wuhan-Hu-1 PV more infectious on a per particle basis, but also more infectious than Alpha, Delta and Omicron which all contain D614G (Fig. 1H). Omicron PV infectivity was significantly lower than other variants tested (Fig. 1H), consistent with reports that Omicron displays reduced infectivity in cell lines commonly used to study SARS-

CoV-2 entry (Meng et al., 2022; Peacock et al., 2022; Shuai et al., 2022; Willett et al., 2022) and in animal models (Shuai et al., 2022). We selected naturally-permissive intestinal epithelial Caco2 cells as targets for PV infection for their endogenous expression of both ACE2 and TMPRSS2 (Thorne et al., 2021). Comparing GBP-restriction of PV infectivity on HeLa-ACE2 cells gave similar results for Wuhan-Hu-1, Wuhan-Hu-1 D614G, Alpha and Delta (Fig, S1J-M). Intriguingly for Omicron, PV made in the presence of GBP2/5 showed enhanced infectivity on HeLa-ACE2 cells (Fig. S1N), that we discuss later.

**GBP2 and 5 inhibition of SARS-CoV-2 spike cleavage**

To define mechanism, we investigated the effects of GBPs on spike S1/S2 cleavage by western blotting. Visualising uncleaved (S) and cleaved spike (S2, S2/S) revealed clear differences in processing of Wuhan-Hu-1 spike on PV particles and in cell lysates in the presence of GBP2 and 5, compared to either no GBPs, or GBP2 C588A and GBP5 C583A mutants (Fig. 2A,B). Quantifying this across all spike variants showed that GBP5 significantly reduced the amount of cleaved spike (lower S2/S ratio) in Wuhan-Hu-1, Alpha, Delta and Omicron PV particles (Fig. 2C). Differential spike cleavage in the presence of GBP5 was also evident in cell lysates, showing decreased S2/S ratios (Fig. 2D), consistent with GBP perturbation of intracellular spike processing. Notably, introducing D614G into Wuhan-Hu-1 increased both the amount of spike incorporated into PV (Fig. 2C, total spike/p24 ratio) and spike expression levels in cell lysates (Fig. 2D). By contrast to Wuhan-Hu-1 D614G spike, Alpha and Delta did not show increased spike expression in cells or greater incorporation into PV compared to WT Wuhan-Hu-1, despite also encoding the D614G substitution. We reasoned that the increase in Wuhan-Hu-1 D614G spike expression and enhanced PV infectivity (Fig. 1H) may also overwhelm GBP restriction, explaining resistance to GBP inhibition (Fig. 1D). Concordantly, lowering the expression of Wuhan-Hu-1 D614G spike by transfecting decreasing amounts of spike plasmid during PV production restored the ability of GBP2/5 to restrict Wuhan-Hu-1 D614G infectivity to levels seen for Wuhan-Hu-1 (Fig. S3A-B). Similarly, decreasing spike expression also sensitised Alpha and Delta PVs to GBP2/5 restriction (Fig. S3C-D), whereas Omicron spike was even further inhibited by GBP2/5 (Fig. S3E). Similar results for Wuhan-Hu-1, Wuhan-Hu-1 D614G, Alpha and Delta PV were obtained when measuring PV infectivity on HeLa ACE2 cells (Fig. S3F-I). Taken together these data show that GBP2 and 5 interfere with spike processing and can restrict SARS-CoV-2 infectivity, but that Alpha and Delta have evolved to escape inhibition, despite showing a GBP-mediated spike cleavage defect, whereas surprisingly Omicron has not.

**Effects of GBP 2 and 5 on spike-mediated cell entry routes**

To test whether GBP-mediated perturbation of spike cleavage in infected cells influences the entry route into target cells, we first confirmed the entry phenotype on Caco2 cells using inhibitors Camostat (a serine protease inhibitor that blocks TMPRSS2) and E64d (an inhibitor of endolysosomal cathepsins) (Fig. 3). It has been shown that early-lineage SARS-CoV-2, and VOCs Alpha and Delta are inhibited by Camostat, but not E64d in cells expressing TMPRSS2, as we confirm here using Caco2 (Fig. 3A-D) (Dicken et al., 2021; Koch et al., 2021; Winstone et al., 2021). By contrast, Omicron was potently inhibited by E64d, and was less sensitive than other SARS-CoV-2 variants to Camostat in both PV and live virus infection assays (Fig. 3A-D), suggesting Omicron more efficiently uses TMPRSS2-independent endosomal entry pathway, concordant with recent studies (Meng et al., 2022; Peacock et al., 2022; Shuai et al., 2022; Willett et al., 2022). Furin-cleavage at S1/S2 can influence viral entry route. Therefore we directly compared Omicron spike S1/S2 cleavage to other VOCs, and early-lineage isolates VIC and IC19, by western blotting viral particles purified from infected Caco2 culture supernatants (Fig. 3E). We found that evolution of VOCs for an optimised FCS correlated, as expected, with cleavage efficiency, with Delta>Alpha>IC19/VIC. Notably, we saw that Omicron virus incorporated predominantly cleaved spike, with little or no uncleaved spike detected in virions (Fig. 3E), a result confirmed using two independent Omicron isolates. Efficient S1/S2 cleavage of Omicron spike is consistent with this VOC containing the FCS optimising mutations P681H, N679K and H655Y (Fig. 1A) that can enhance S1/S2 cleavage (Escalera et al., 2022; Peacock et al., 2021b). The total amount of cleaved spike in virions (S2/N) was however lower for Omicron compared to other VOCs (Fig. 3E). These data suggest that Omicron's shift in cellular tropism is unlikely to be explained by inefficient spike cleavage in virions.

Next we tested whether inhibition of furin-mediated spike cleavage by GBPs influences the entry pathway of SARS-CoV-2, potentially redirecting entry away from TMPRSS2 dependence and fusion at the plasma membrane and towards endosomal cathepsin-dependent fusion (Fig. 3F-H). We found GBP2 and 5 partially, but significantly, sensitised Wuhan-Hu-1 PV to inhibition by E64d, but not Camostat, on Caco2 cells (Fig. 3H). For Omicron, addition of E64d, but not Camostat, further reduced infection of PV made in the presence of GBP5 (Fig. 3I,J). Together, these data suggest that GBP-mediated inhibition of spike cleavage can lead to increased endosomal entry, but that it does not make virus completely TMPRSS2-independent. HeLa-ACE2 cells support more endocytic entry of SARS-CoV-2, evidenced by E64d, but not Camostat, inhibiting infection of IC19, VIC, Alpha and Delta viruses on HeLa-ACE2 (Fig. S4). Consistent with this, GBP5 restricted Wuhan-Hu-1 PV infection of HeLa-ACE2 cells, however Omicron PV infection was instead

enhanced on HeLa-ACE2, and not restricted on 293T-ACE2 cells (Fig. S5), concordant with Omicron's use of endocytic entry routes.

**The interplay between GBP and IFITM restriction**

IFITMs can target SARS-CoV-2 spike fusion with host cell membranes to inhibit viral infection (Buchrieser et al., 2020; Lista et al., 2021; Martin-Sancho et al., 2021; Peacock et al., 2021a; Shi et al., 2021; Winstone et al., 2021). IFITMs are differentially localised in cells, with IFITM1 being found mostly at the plasma membrane and IFITM2/3 predominantly endosomal. Viral entry route influences IFITM restriction, with mutations in the FCS that promote endosomal uptake of SARS-CoV-2 increasing sensitivity to IFITM2 (Lista et al., 2021; Winstone et al., 2021). Having shown that GBPs perturb furin cleavage of spike, partially redirecting PV towards endosomal entry, we investigated whether GBPs sensitise PV to endosomal IFITM restriction. To do this we used Caco2 cells stably expressing either IFITM1, 2 or 3 (Fig. 4A), confirming the expected IFITM localisation by immunofluorescence microscopy (Fig. 4B). Consistent with TMPRSS2-dependent plasma membrane entry, IFITM1 potently and significantly inhibited infection of early-lineage viruses (VIC, IC19) and VOCs Alpha and Delta in Caco2 cells (Fig. 4C-F). By contrast, IFITM2 and IFITM3 did not inhibit, but rather enhanced, infection by these viruses (Fig. 4C-F), in agreement with previous studies (Buchrieser et al., 2020; Lista et al., 2021; Nchioua et al., 2021; Prelli Bozzo et al., 2021; Winstone et al., 2021). Similar results were obtained using PV infection assays (Fig. 4H-K). Preventing TMPRSS2-mediated entry with Camostat sensitised Wuhan-Hu-1 PV to IFITM2 and 3 inhibition, leading to an almost complete block to infection by redirecting entry towards endosomes and exposing to IFITM2/3 (Fig. 4M). Testing GBP5-mediated inhibition of spike cleavage on the sensitivity of PV to IFITMs (Fig. 4N-Q), we found no significant difference in IFITM-1 inhibition of Wuhan-Hu-1 PV made in the presence or absence of GBP5. Moreover, for IFITM2/3 although PV made in the presence of GBP5 appeared to show enhanced sensitivity to IFITM2/3, this effect can be accounted for largely by the inhibitory effect of GBP5, evidenced by comparing infectivity of GBP5 with IFITM2 or 3, to GBP5 alone. Moreover, Wuhan-1 D614G, Alpha and Delta PV sensitivity to IFITMs was similarly unaffected by GBP (Fig. 4N-Q). Collectively these data show that while combining GBPs and IFITMs can lead to an overall potent reduction of infection, inhibiting furin cleavage by GBPs does not make a virus that is resistant to IFITMs become "sensitised" to IFITM restriction. Given that GBPs did not completely prevent S1/S2 spike cleavage in our pseudovirus assay, this result is not unexpected.

**Omicron virus is restricted by IFITM 1, 2 and 3**

The recently emerged Omicron variant has acquired over 30 spike mutations compared to Wuhan-Hu-1 (Fig. 1A). Having shown that Omicron was sensitive to GBP inhibition, we next tested Omicron's sensitivity to IFITMs. Strikingly, we found Omicron was unique amongst SARS-CoV-2 viruses, being sensitive to inhibition of infection by IFITM1, 2 and 3 in Caco2 cells (Fig. 4G). Similar restriction of Omicron by IFITM1, 2 and 3 was seen in PV assays (Fig. 4L). Next we investigated the effects of combining GBP and IFITMs on Omicron infection. Fig. 4R shows that Omicron PV made in the presence of GBP5 was not significantly more sensitive to IFITM restriction, despite GBP proteins inhibiting Omicron PV infectivity similar to Wuhan-Hu-1. The spike cytoplasmic tail of SARS-CoV-2 contains an endoplasmic reticulum (ER)-retention signal, hence truncation of the last 19 resides of the spike cytoplasmic tail (ΔCT) has been shown to boost spike incorporation and particle infectivity during pseudotyping (Ou et al., 2020; Schmidt et al., 2020). Indeed, PV containing the Omicron ΔCT spike showed a 70-fold increase in infectivity (Fig. 5A). However, we found no difference in the magnitude of GBP5 restriction of Omicron PV containing ΔCT spike compared to full-length spike (Fig. 5B), and no rescue from restriction by IFITMs (Fig. 5C-F). Taken together, data reveal key differences between Omicron and preceding SARS-CoV-2 variants in their sensitivity to endosomal IFITM restriction factors, indicative of an altered Omicron entry route.

**Discussion**

Innate immunity is a potent first-line host cell defence against viruses, upregulating a group of interferon-stimulated genes (ISGs) which can act directly as antiviral restriction factors, targeting key steps in viral replication and collectively inducing an antiviral state. SARS-CoV-2 activates innate immune sensing and induces an interferon-response (Lei et al., 2020; Thorne et al., 2022; Thorne et al., 2021), upregulating canonical ISGs including GBP2 and 5 in human airway epithelial cells (Ziegler et al., 2020). In this study we show that the interferon-inducible restriction factors GBP2 and 5 interfere with furin-mediated cleavage of SARS-CoV-2 spike and potently inhibit infection by the early-lineage SARS-CoV-2 strain Wuhan-Hu-1. We also report the differential sensitivity of VOC spikes to GBP and IFITM restriction. Using spikes from other coronaviruses with pandemic potential, MERS-CoV and SARS-CoV-1, we show that restriction by GBP2/5 correlates with the differential requirement for furin-mediated spike processing, such that MERS-CoV spike is sensitive, but SARS-CoV-1 resistant, to inhibition by GBP.

We have previously shown that evolution of mutations outside of spike allow for SARS-CoV-2 evasion/antagonism of innate immune sensing (Thorne et al., 2022); however, spike itself can be targeted by innate immune responses, in the form of GBPs that we show here, and IFITM proteins. Alpha and Delta have both evolved an optimised FCS, leading to enhanced S1/S2 spike cleavage (Escalera et al., 2022; Lista et al., 2021; Peacock et al., 2021b), with other mutations outside the FCS (i.e. H69/V70 deletion and D614G) also influencing spike cleavage (Escalera et al., 2022; Gobeil et al., 2021; Meng et al., 2021). Therefore, we hypothesised that evolution of these VOCs may have led to, or selected for, evasion from GBPs that we show potently inhibit early-lineage Wuhan-Hu-1. However, while Alpha and Delta were resistant to GBP-mediated inhibition of PV infectivity, they both displayed the GBP-mediated spike cleavage defect similar Wuhan-Hu-1. Escape from GBP restriction by these VOC spikes in our PV assay cannot therefore be simply attributed to an optimised FCS overcoming GBP inhibition of spike S1/S2 cleavage. Moreover, Omicron PV infectivity was potently inhibited by GBP2/5, despite also containing the same FCS-optimising mutations as other VOC. Instead, we propose that evolution of Alpha and Delta for enhanced activity of spike, including better fusogenicity and infectivity (Johnson et al., 2021; Peacock et al., 2021a; Rajah et al., 2021; Saito et al., 2022), are likely key determinants mediating escape from GBP restriction. In support, we find a correlation between inherent PV infectivity and the GBP restriction phenotype, such that Alpha and Delta, which are more infectious on Caco2 cells, escape restriction, whereas less infectious Wuhan-Hu-1 and Omicron, are restricted (Meng et al., 2022; Peacock et al., 2022; Rajah et al., 2021; Saito et al., 2022). Consistent with the notion that enhanced infectivity contributes to escape from GBPs, introducing the D614G substitution into Wuhan-Hu-1 increased PV infectivity and spike incorporation, and rescued Wuhan-Hu-1 from restriction. However Alpha and Delta PV resistance to GBPs is not due to increased spike in PV particles. This is because the amount of cleaved spike in PV was comparable between Wuhan-Hu-1 (restricted) and Alpha and Delta (not-restricted). Furthermore, for Omicron, increasing the amount of incorporated spike into PVs did not overcome GBP restriction or rescue infection. Therefore, we propose that it is the combined effects of mutations that have accumulated in Alpha and Delta spikes, changing spike activity and infectivity, that have led to evolution of these VOCs to escape inhibition by GBPs.

IFITMs are another family of ISGs that can target SARS-CoV-2 spike and restrict infection, in this case by inhibiting fusion of viral and cellular membranes. Consistent with early-lineage Wuhan-Hu-1/VIC/IC19, and Alpha and Delta viruses preferentially infecting by plasma membrane fusion, we found that IFITM1, but not IFITM2 and 3, inhibited infection of Caco2 cells, naturally-permissive intestinal epithelial cells that endogenously express ACE2

and TMPRSS2 (Koch et al., 2021; Thorne et al., 2021). Mutation of the FCS can alter the route of SARS-CoV-2 entry and sensitise virus to inhibition by endosomal IFITM (Lista et al., 2021; Winstone et al., 2021). Concordantly, we found inhibiting plasma membrane entry with Camostat, and redirecting entry towards a more endosomal pathway, led to restriction of Wuhan-Hu-1 by IFITM2 and 3. However, although GBP inhibition of spike cleavage resulted in increased sensitivity to E64d (indicative of increased endosomal entry), GBPs did not sensitise Wuhan-Hu-1 PV to inhibition by endosomal IFITM2 or 3. We explain this by GBPs reducing, but not completely preventing, spike S1/S2 cleavage in our PV assay, allowing for a significant proportion of PV particles to use TMPRSS2-dependent plasma membrane fusion, avoiding endosomal IFITM restriction. It is notable therefore, that combining GBP5 in producer cells, with IFITM1 in target cells, led to an almost complete inhibition of Wuhan-Hu-1 infection, when compared to infection in the absence of these restriction factors. Thus, during an innate immune response to viral infection, where multiple ISGs, including GBP2/5 and IFITM1/2/3 are induced, we might expect to see stronger inhibitory effects.

Our most striking observation is that Omicron is unique amongst the VOCs we tested in being sensitive to inhibition by GBP2/5, and also IFITM1, 2 and 3. Omicron is also unique amongst SARS-CoV-2 in its entry pathway, evolving towards TMPRSS2-independent fusion (Meng et al., 2022; Peacock et al., 2022; Willett et al., 2022). In agreement with these recent reports, we also show Omicron is less sensitive to the TMPRSS2 inhibitor Camostat, while being more sensitive to the cathepsin inhibitor E64d, and significantly less infectious than other SARS-CoV-2 isolates on TMPRSS2 expressing Caco2 cells. Omicron's use of an endosomal entry pathway is consistent with our observation that, unlike other VOCs, Omicron is sensitive to inhibition by IFITM2 and 3, which are predominantly located within endosomes. Because Omicron contains the same P681H FCS-optimising mutation as Alpha, and has enhanced affinity for ACE2 that is also seen for Alpha and Delta (Meng et al., 2022; Peacock et al., 2022; Rajah et al., 2021; Willett et al., 2022), we expected that Omicron would be resistant to GBPs in our PV assay, similar to the other VOCs. However, Omicron was surprisingly sensitive to GBP2/5, behaving like Wuhan-Hu-1. Moreover, increasing Omicron spike incorporation into PV did not rescue from GBP or IFITM restriction. Collectively, these data suggest that inherent changes to Omicron's spike activity, compared to other VOCs, rather than differences in spike incorporation or S1/S2 cleavage efficiency, make Omicron sensitive to GBP-mediated restriction. Omicron spike is reportedly less fusogenic (Meng et al., 2022; Peacock et al., 2022; Willett et al., 2022), and slowing down of the fusion process is a plausible mechanism explaining Omicron's sensitivity to restriction by GBP2/5 and IFITM1/2/3, that interfere with viral fusion and cell entry. Intriguingly, compared to Wuhan-Hu-1, Omicron contains 3 unique mutations (Q954H, N969K and L981F) within

the heptad repeat domain 1 (HR1) of spike that mediates viral fusion, as well as N856K adjacent to the fusion peptide (Fig. 1A) (Meng et al., 2022; Xia et al., 2020). These substitutions are not in Alpha and Delta, and so we speculate that they may contribute to the differences between Omicron and other VOCs in spike fusion, sensitivity to restriction and tropism. Given the significant number of substitutions in Omicron, it is likely that the situation will be more complex, and that changes in and around the RBD, NTD and S1/S2 cleavage junction may also contribute to the Omicron phenotype. The *in vivo* interplay between Omicron and innate immunity, restriction factors and tropism remains unknown. It is possible that the expression of different innate immune restriction factors varies across cells/tissues, such that Omicron has evolved into a niche that allows it to avoid or tolerate GBPs and IFITMs. Moreover, IFITM2 and 3 are suggested to act as co-factors for SARS-CoV-2 in some cases (Prelli Bozzo et al., 2021), and we and others also see enhancement of early-lineage isolates and Alpha and Delta infection by IFITM2/3 (Buchrieser et al., 2020; Lista et al., 2021; Nchioua et al., 2021; Prelli Bozzo et al., 2021; Winstone et al., 2021), so it cannot be excluded that Omicron may similarly exploit IFITMs in some settings. It is clear that SARS-CoV-2 needs to balance efficient cell entry with evasion of compartmentalised restriction factors, and it will be intriguing to see how Omicron does this, and precisely how it infects target cells. Omicron has evidently evolved to do things differently, but effectively, and exploit a different cellular niche, one to which it is clearly well-adapted.

SARS-CoV-2 VOCs have evolved separately from ancestral wave one strains and not from each other. It is therefore not surprising that these VOCs have explored different evolutionary solutions to the problems they faced, and that the selective pressures encountered by each VOC are not identical. For example, Alpha and Delta evolved prior to significant levels of adaptive immunity in the population, thus these VOCs may have faced stronger pressure to evolve spikes that evade innate immunity, including restriction factors like GBPs and IFITMs, while being less influenced by the need for humoral immune escape. By contrast Omicron, the first real antibody escape variant, evolved at a time of much greater population level humoral immunity, therefore Omicron has been exposed to different selective pressures, requiring different evolutionary solutions. Our data showing differential sensitivity of Alpha/Delta vs Omicron to GBP and IFITM restriction, as well as others showing significant Omicron antibody escape (Meng et al., 2022; Willett et al., 2022), are consistent with this, reinforcing the notion that Omicron has taken a different evolutionary path to preceding VOCs. We propose a scenario in which evolution of Omicron spike for neutralising antibody escape has influenced the ability to evade innate immunity. The critical balance between viral evasion of innate and adaptive immunity has precedent. This is a borne out of studies of HIV-1 evolution in host, where HIV-1 isolates from early in infection

(so called transmitter/founder viruses) are completely resistant to IFITM restriction, but overtime, the selective pressure from adaptive immunity, and the resulting neutralising antibody escape mutations in HIV-1 Env, leads to viral isolates having increased sensitivity to IFITMs and interferons (Foster et al., 2016). We propose that similar processes have occurred during SARS-CoV-2 evolution to host, in which the need to escape from neutralising antibody became the dominant selective pressure on Omicron, resulting in a compensatory, but tolerable, increase in sensitivity to innate immunity, while also impacting on spike activity and cell tropism. We predict that this interplay between evasion of innate and adaptive immunity, and the consequences for transmission and tropism, will be features of future SARS-CoV-2 evolution, and emergence of new VOCs, and that linking this evolution to phenotype will become important aspects for understanding and predicting SARS-CoV-2 biology and ultimately pathogenesis.

## Materials and methods

### Cells

HEK293T/17 cells (abbreviated herein as 293T cells) were obtained from American Type Culture Collection (ATCC, CRL-11268). Caco2 cells were a gift from Dalan Bailey (Pirbright Institute) and originally obtained from ATCC. HeLa-ACE2 (stable cell line expressing ACE2) were provided by J.E. Voss and D. Huang (Scripps Research Institute) (Rogers et al., 2020). Vero.E6 cells were obtained from the National Institute for Biological Standards and Control (NIBSC). Vero.E6-TMPRSS2 cells (stable cell line expressing TMPRSS2 under G418 selection) were a gift from Mala Maini (UCL). 293T-ACE2 (stable cell line expressing ACE2 under puromycin selection) were a gift from Wendy Barclay (Imperial College London). HeLa-TZM-bl cells (expressing luciferase and beta-galactosidase under the control of HIV-1 LTR) were obtained from the Centre for AIDS Reagents (CFAR). All cell lines were grown in Dulbecco's modified Eagle's medium (DMEM, Thermo Fisher Scientific) supplemented with 10% foetal calf serum (Labtech) and 1% Pen Strep (penicillin-streptomycin, Thermo Fisher Scientific), and maintained in humidified 5% CO2 incubators at 37°C. Cells were passaged every 2-4 days when they reached 80-90% confluency. Caco2 cells were transduced with IFITM1/2/3 lentivectors as described previously (Petrillo et al., 2018) and selected with 10 µg/ml puromycin (Merck) to produce stable cell lines expressing individual HA-tagged IFITM proteins. IFITM expression was confirmed by flow cytometry.

**Plasmids**

SARS-CoV-2 Spike expression vectors were originally synthesised by Genewiz and subcloned into pCDNA3.1+ vector. All spike sequences are full-length, unless otherwise stated. Wuhan-Hu-1 WT (Seow et al., 2020), Wuhan-Hu-1 D614G (Kemp et al., 2021) and Alpha (Rees-Spear et al., 2021) spike expression vectors were gift from Laura McCoy (UCL). Delta and Omicron spike expression vectors were a gift from Katie Doores (King's College London). Omicron spike ΔCT expression vector was a gift from Wendy Barclay (Imperial College London). SARS-CoV-1 Spike and MERS-CoV Spike expression vectors were a gift from Joe Grove (Centre for Virus Research, Glasgow). Plasmid encoding HIV-1 Env pSVIII_JRFL was a gift from Laura McCoy (UCL). Plasmid encoding full length HIV-1 pNL4.3 was donated by Dr M Martin and obtained from CFAR. Lentiviral backbone packaging plasmid (expressing HIV Gag, Pol, Tat and Rev) p8.91 and the reporter plasmid encoding luciferase gene pCSLW were a gift from Greg Towers (UCL). GBP expression vectors encoding HA-tagged GBPs (GBP2 WT, GBP2 C588A, GBP5 WT, GBP5 C583A) and BFP reporter expressed from an IRES (Braun et al., 2019; Krapp et al., 2016) were a gift from Daniel Sauter (Ulm University Medical Center, Germany).

**SARS-CoV-2 viruses**

SARS-CoV-2 isolates VIC (BetaCoV/Australia/VIC01/2020, lineage B), IC19 (hCoV-19/England/IC19/2020, lineage B.1.13) and Alpha (hCoV-19/England/204690005/2020, lineage B.1.1.7) have been described previously (Thorne et al., 2022). SARS-CoV-2 Delta (lineage B.1.617.2) and Omicron (lineage B.1.1.529/BA.1) isolates were a kind gift from Wendy Barclay (Imperial College London, UK) (Peacock et al., 2022; Peacock et al., 2021b). Viruses were propagated by infecting Caco2 cells at MOI 0.01 TCID50 per cell, in DMEM culture medium supplemented with 1% FCS and 1% penicillin/streptomycin, at 37 °C. Virus was collected at 72 hpi and clarified by centrifugation at 2100xg for 15 min at 4 °C to remove any cellular debris. Virus stocks were aliquoted and stored at −80°C. Virus stocks were quantified by extracting RNA from 100 µl of supernatant with 1 µg carrier RNA using Qiagen RNeasy clean-up RNA protocol, before measuring viral E RNA copies per ml by RT-qPCR as described previously (Thorne et al., 2021).

**Live virus infections**

For infections, Caco2 ($1x10^5$ cells/well) and HeLa-ACE2 ($6.5x10^4$ cells/well) were seeded in 24-well plates one day before infection. Cells were infected with 1000 E RNA copies per cell in 200ul culture medium. After 2h incubation at 37°C, cells were carefully washed with PBS to remove excess virus and fresh culture medium was added. For inhibition assays, cells were pre-treated with inhibitors at the indicated concentrations for 2h prior to infections and

maintained throughout the experiment. At the indicated time points, cells were collected for analysis.

**Pseudovirus production**

Spike pseudoviruses (PVs) were made by co-transfection of spike, p8.91 and pCSLW plasmids as described previously (Dicken et al., 2021). To determine GBP inhibition, PV plasmids were transfected together with GBP vector or empty vector (EV) control expressing only BFP reporter. Briefly, $5x10^4$ 293T cells were seeded onto 24-well plates for 24h and then transfected with 260 ng p8.91, 260 ng pCSLW, 40 ng spike and 20-120 ng GBP vectors or EV control using Fugene6 (Promega). For larger scale production cells were seeded in 6-well plates with cell numbers and transfection reagents scaled up five-fold. For HIV-1 Env PV, 293T cells were seeded as described above and transfected with 240 ng p8.91, 240 ng pCSLW,120 ng pSVIII-JRFL Env and indicated doses of GBP or empty vector control.
PV supernatants were collected at 48 and 72 h post-transfection and purified through centrifuge-driven 0.45 µm filter units (Corning) or syringe-driven 0.45 µm filter units (Starlab) and used within 24h without freeze-thawing. The amount of PV in the supernatant was determined by measuring the supernatant RT activity using SYBR-green–based product enhanced reverse transcription assay (SG-PERT) by qPCR, performed as described previously (Pizzato et al., 2009).

**Pseudovirus infection**

Target cells were seeded into white 96-well plates 24h before infection (Caco2, Vero.E6 and Vero.E6-TMPRSS2 cells seeded at $1.5x10^4$ cells/well, 293T-ACE2, HeLa-ACE2 and HeLa-TZMbl cells seeded at $1x10^4$ cells/well). Cells were infected equal doses (25 µl) of PV supernatant and incubated at 37°C for 48 h without changing the media. Luciferase expression (RLU) was measured at 48 h post-infection using BrightGlo substrate (Promega) according to manufacturer's instruction on Glomax luminometer (Promega). For inhibitor studies cells were pre-treated before infections for 2 h with Camostat mesylate (Apexbio, 0.2-100 µM) or E64d (Focus Biomolecules, 0.2-25 µM). To obtain infectivity (RLU/RT) values, RLU values were normalised to supernatant RT activity (measured by SG-PERT assay).

**HIV-1 infection**

293T cells were seeded in 24-well plates as described above and transfected with 120ng pNL4.3 and indicated doses of GBP or empty vector control using Fugene6 to produce infectious HIV-1 virus in presence or absence of GBPs. Virus-containing supernatant was harvested and RT activity measured as described above. HeLa-TZMbl were seeded into

white 96-well plates 24h before infection ($1x10^4$ cells/well) and infected with 10 µl of virus supernatant/well. Luciferase activity was measured 48 h post-infection as described above.

**GBP inhibition assay**

Spike PV, HIV-1 Env PV or HIV-1 virus were made in presence of increasing doses of GBP2/5 or their mutants or empty vector control as described above. Supernatant RT activity (RT units) was measured by SG-PERT assay to determine PV or virus content in supernatants. As indicated, different cell lines were infected with equal doses of PV/virus supernatants for 48 h and luciferase expression (RLU) was measured as describe above. Infectivity of the supernatant was determined as a ratio of RLU to RT units (RLU/RT) and normalised to empty vector control (no GBP), set at 100% for each PV or virus.

**IFITM inhibition assay**

Caco2 cells, WT or stably expressing IFITM1/2/3 (described above), were infected with indicated spike PVs and luciferase expression was measured 48 h post-infection as described above. Infectivity (RLU/RT) was normalised to Caco2 WT control (100%). Alternatively, spike PV were made in presence of GBP5 or EV control and used to infect Caco2 WT and IFITM expressing cells. Infection of Caco2-IFITM1/2/3 cells with live SARS-CoV-2 virus was done as described above.

**Immunoblotting**

PV were concentrated and purified from the supernatant by centrifugation (2h 13,000g, $4^0$C) through a 20% sucrose cushion and resuspended in 20 µl Leammli buffer. Cells were harvested at 48h post-transfection, lysed in RIPA buffer and protein concentration determined by the BCA assay (Thermo Fisher Scientific). Twenty micrograms of cell lysate and an equal volume of purified virus were separated by SDS-PAGE, transferred to nitrocellulose membrane and membranes probed using the following primary antibodies: anti-SARS-CoV Spike (100% overlap with the SARS-CoV-2 epitope) (Invitrogen, PA1-41165, 1:1000), anti SARS-CoV nucleoprotein (N) monoclonal antibody (clone CR3009, gift from Laura McCoy, 0.5 µg/ml), anti-HA-tag (Biolegend, 16B12, 1:2000), anti-Gag p24 (CFAR, ARP432, 1:2000) and anti-tubulin (Sigma, DM1A, 1:1000). Primary antibodies were incubated overnight at 4°C with agitation and detected with fluorescent secondary antibodies: anti-Rabbit IgG (IRDye 800CW, Abcam, ab216773, 1:10,000), anti-Mouse IgG (IRDye 680RD, Abcam, ab216776, 1:10,000) and anti-Human IgG (IRDye 800CW, Licor, 925-68078, 1:10,000), and imaged with an Odyssey Cxl Infrared Imager (Licor). Immunoblots were analysed with Image Studio Lite software.

**Flow cytometry**

Cells were harvested and detached with Trypsin-EDTA (Thermo Fisher Scientific), stained with Zombie NIR live-dead dye (Biolegend) in PBS (1:500, 5min), washed and fixed with 4% formaldehyde (Sigma) for 20-30 min at RT. Cells infected with live SARS-CoV-2 virus were fixed with 4% formaldehyde for 1h at RT. Cells were then washed and permeabilised with Perm buffer (Biolegend) for 5 min at RT and stained with primary antibodies (20 min at RT): anti-HA-tag-APC (Biolegend, 16B12, 1:150), anti-Gag-PE (Beckam Coulter, KC57, 1:250). SARS-CoV-2 infection was detected by intracellular staining for nucleoprotein (N) using anti-SARS-CoV N monoclonal antibody (human, clone CR3009, gift from Laura McCoy, 1 µg/ml) and secondary anti-Human IgG-AF488 (Jackson labs, 1:400). For analysis of cell surface spike infection, 293T cells were harvested with 5 mM EDTA (Sigma), washed, stained with Zombie NIR and anti-SARS-CoV-2 Spike antibody from human convalescent sera (NIBSC, 20/130 1:200) on ice for 30 min. Primary antibodies were detected with the secondary anti-Human IgG-AF488 before fixation and intracellular stain as described above.

**Immunofluorescence Microscopy**

Caco2 cells were fixed in 4%PFA (Sigma) for 15 minutes, followed by permeabilisation in 0.25%Triton-TX100 (Sigma) for 15 minutes. A blocking step was carried out for 1h at room temperature with 1%BSA (Sigma) and 0.1% Triton TX100 in PBS. Primary antibody incubation was carried out for 1h at RT with rabbit anti-HA antibody (H6908, Sigma-Aldrich) to label IFITM1, IFITM2 and IFITM3 and mouse anti-CD63 (IB5, a gift from M. Marsh, UCL) to label endogenous CD63. Primary antibodies were detected with secondary anti-rabbit AlexaFluor-488 and anti-mouse AlexaFluor-568 conjugates (Jackson Immuno Research) for 1h. All cells were labelled with Hoechst33342 (H3570, Thermo Fisher). Images were acquired using the WiScan® Hermes 7-Colour High-Content Imaging System (IDEA Bio-Medical, Rehovot, Israel) at magnification 40X/0.75NA. Three channel automated acquisition was carried out sequentially. Scale bars and RGB composite images were created in in FIJI ImageJ software package (Schindelin et al., 2012).

**Statistical Analysis**

Statistical significance was calculated using Prism 9 (GraphPad Prism) using indicated statistical tests and significance was assumed when $P < 0.05$.

**Acknowledgements**

This work was funded by Wellcome Investigator Award 108079 followed by 223065 to C.J. G.J.T. was funded by Wellcome Senior Fellowship 108183 followed by Wellcome Investigator Award 220863. C.J. and G.J.T. were also funded by MRC/UKRI G2P-UK

National Virology consortium (MR/W005611/1) and the UCL COVID-19 fund. We thank the G2P-UK National Virology Consortium; W. Barclay at Imperial College London, UK; G. Screaton Oxford University, UK; Dalan Bailey at Pirbright Institute UK; Laura McCoy at University College London UK; J.E. Voss and D. Huang at Scripps Research Institute USA; Joe Grove at the Centre for Virus Research, Glasgow, UK; Katie Doores at King's College London UK, and Daniel Sauter at Ulm University Medical Center, Ulm Germany for provision of reagents and variant isolates. We also acknowledge members of the G2P-UK Consortium, as well as the Jolly lab and Towers lab for helpful discussions.

**Author contributions**

C.J. conceived the study. D.M., A-K.R., M.X.V.W., T.B., T.H., and L.T., performed the experiments and analysed the data. D.M., A-K.R., and C.J. wrote the manuscript with contributions from all authors.

**References**

Boni, M.F., Lemey, P., Jiang, X., Lam, T.T.-Y., Perry, B.W., Castoe, T.A., Rambaut, A., and Robertson, D.L. (2020). Evolutionary origins of the SARS-CoV-2 sarbecovirus lineage responsible for the COVID-19 pandemic. Nat Micro *5*, 1408-1417.

Braun, E., Hotter, D., Koepke, L., Zech, F., Groß, R., Sparrer, K.M.J., Müller, J.A., Pfaller, C.K., Heusinger, E., Wombacher, R.*, et al.* (2019). Guanylate-Binding Proteins 2 and 5 Exert Broad Antiviral Activity by Inhibiting Furin-Mediated Processing of Viral Envelope Proteins. Cell Rep *27*, 2092-2104.e2010.

Buchrieser, J., Dufloo, J., Hubert, M., Monel, B., Planas, D., Rajah, M.M., Planchais, C., Porrot, F., Guivel-Benhassine, F., Van der Werf, S.*, et al.* (2020). Syncytia formation by SARS-CoV-2-infected cells. EMBO J *39*, e106267.

Dicken, S.J., Murray, M.J., Thorne, L.G., Reuschl, A.-K., Forrest, C., Ganeshalingham, M., Muir, L., Kalemera, M.D., Palor, M., McCoy, L.E.*, et al.* (2021). Characterisation of B.1.1.7 and Pangolin coronavirus spike provides insights on the evolutionary trajectory of SARS-CoV-2. bioRxiv, 2021.2003.2022.436468.

Du, X., Tang, H., Gao, L., Wu, Z., Meng, F., Yan, R., Qiao, S., An, J., Wang, C., and Qin, F.X.-F. (2022). Omicron adopts a different strategy from Delta and other variants to adapt to host. Signal Transduction and Targeted Therapy *7*, 45.

Escalera, A., Gonzalez-Reiche, A.S., Aslam, S., Mena, I., Laporte, M., Pearl, R.L., Fossati, A., Rathnasinghe, R., Alshammary, H., van de Guchte, A.*, et al.* (2022). Mutations in SARS-CoV-2 variants of concern link to increased spike cleavage and virus transmission. Cell Host Microbe. Online ahead of print doi: 10.1016/j.chom.2022.01.006.

Foster, T.L., Wilson, H., Iyer, S.S., Coss, K., Doores, K., Smith, S., Kellam, P., Finzi, A., Borrow, P., Hahn, B.H.*, et al.* (2016). Resistance of Transmitted Founder HIV-1 to IFITM-Mediated Restriction. Cell Host Microbe *20*, 429-442.

Gobeil, S.M., Janowska, K., McDowell, S., Mansouri, K., Parks, R., Manne, K., Stalls, V., Kopp, M.F., Henderson, R., Edwards, R.J.*, et al.* (2021). D614G Mutation Alters SARS-CoV-2 Spike Conformation and Enhances Protease Cleavage at the S1/S2 Junction. Cell Rep *34*, 108630.

Guo, K., Barrett, B.S., Mickens, K.L., Vladar, E.K., Morrison, J.H., Hasenkrug, K.J., Poeschla, E.M., and Santiago, M.L. (2021). Interferon Resistance of Emerging SARS-CoV-2 Variants. bioRxiv, 2021.2003.2020.436257.

Hoffmann, M., Kleine-Weber, H., and Pöhlmann, S. (2020a). A Multibasic Cleavage Site in the Spike Protein of SARS-CoV-2 Is Essential for Infection of Human Lung Cells. Mol Cell *78*, 779-784.e775.

Hoffmann, M., Kleine-Weber, H., Schroeder, S., Kruger, N., Herrler, T., Erichsen, S., Schiergens, T.S., Herrler, G., Wu, N.H., Nitsche, A.*, et al.* (2020b). SARS-CoV-2 Cell Entry Depends on ACE2 and TMPRSS2 and Is Blocked by a Clinically Proven Protease Inhibitor. Cell *181*, 271-280 e278.

Hotter, D., Sauter, D., and Kirchhoff, F. (2017). Guanylate binding protein 5: Impairing virion infectivity by targeting retroviral envelope glycoproteins. Small GTPases *8*, 31-37.

Jackson, C.B., Farzan, M., Chen, B., and Choe, H. (2022). Mechanisms of SARS-CoV-2 entry into cells. Nat Rev Mol Cell Biol *23*, 3-20.

Johnson, B.A., Xie, X., Bailey, A.L., Kalveram, B., Lokugamage, K.G., Muruato, A., Zou, J., Zhang, X., Juelich, T., Smith, J.K.*, et al.* (2021). Loss of furin cleavage site attenuates SARS-CoV-2 pathogenesis. Nature *591*, 293-299.

Kemp, S.A., Collier, D.A., Datir, R.P., Ferreira, I., Gayed, S., Jahun, A., Hosmillo, M., Rees-Spear, C., Mlcochova, P., Lumb, I.U.*, et al.* (2021). SARS-CoV-2 evolution during treatment of chronic infection. Nature *592*, 277-282.

Koch, J., Uckeley, Z.M., Doldan, P., Stanifer, M., Boulant, S., and Lozach, P.-Y. (2021). TMPRSS2 expression dictates the entry route used by SARS-CoV-2 to infect host cells. EMBO J *40*, e107821.

Korber, B., Fischer, W.M., Gnanakaran, S., Yoon, H., Theiler, J., Abfalterer, W., Hengartner, N., Giorgi, E.E., Bhattacharya, T., Foley, B.*, et al.* (2020). Tracking Changes in SARS-CoV-2 Spike: Evidence that D614G Increases Infectivity of the COVID-19 Virus. Cell *182*, 812-827.e819.

Krapp, C., Hotter, D., Gawanbacht, A., McLaren, P.J., Kluge, S.F., Stürzel, C.M., Mack, K., Reith, E., Engelhart, S., Ciuffi, A.*, et al.* (2016). Guanylate Binding Protein (GBP) 5 Is an Interferon-Inducible Inhibitor of HIV-1 Infectivity. Cell Host Microbe *19*, 504-514.

Lei, X., Dong, X., Ma, R., Wang, W., Xiao, X., Tian, Z., Wang, C., Wang, Y., Li, L., Ren, L.*, et al.* (2020). Activation and evasion of type I interferon responses by SARS-CoV-2. Nat Commun *11*, 3810.

Lista, M.J., Winstone, H., Wilson, H.D., Dyer, A., Pickering, S., Galao, R.P., De Lorenzo, G., Cowton, V.M., Furnon, W., Suarez, N.*, et al.* (2021). The P681H mutation in the Spike glycoprotein confers Type I interferon resistance in the SARS-CoV-2 alpha (B.1.1.7) variant. bioRxiv, 2021.2011.2009.467693.

Martens, S., and Howard, J. (2006). The interferon-inducible GTPases. Annu Rev Cell Dev Biol *22*, 559-589.

Martin-Sancho, L., Lewinski, M.K., Pache, L., Stoneham, C.A., Yin, X., Becker, M.E., Pratt, D., Churas, C., Rosenthal, S.B., Liu, S.*, et al.* (2021). Functional landscape of SARS-CoV-2 cellular restriction. Mol Cell *81*, 2656-2668.e2658.

Meng, B., Abdullahi, A., Ferreira, I.A.T.M., Goonawardane, N., Saito, A., Kimura, I., Yamasoba, D., Gerber, P.P., Fatihi, S., Rathore, S.*, et al.* (2022). Altered TMPRSS2 usage

by SARS-CoV-2 Omicron impacts tropism and fusogenicity. Nature. Online ahead of print DOI: 10.1038/s41586-022-04474-x

Meng, B., Kemp, S.A., Papa, G., Datir, R., Ferreira, I., Marelli, S., Harvey, W.T., Lytras, S., Mohamed, A., Gallo, G.*, et al.* (2021). Recurrent emergence of SARS-CoV-2 spike deletion H69/V70 and its role in the Alpha variant B.1.1.7. Cell Rep *35*, 109292.

Millet, J.K., and Whittaker, G.R. (2014). Host cell entry of Middle East respiratory syndrome coronavirus after two-step, furin-mediated activation of the spike protein. Proc Natl Acad Sci U S A *111*, 15214-15219.

Nchioua, R., Schundner, A., Kmiec, D., Prelli-Bozzo, C., Zech, F., Koepke, L., Graf, A., Krebs, S., Blum, H., Frick, M.*, et al.* (2021). SARS-CoV-2 variants of concern remain dependent on IFITM2 for efficient replication in human lung cells. bioRxiv, 2021.2011.2017.468942.

Ou, X., Liu, Y., Lei, X., Li, P., Mi, D., Ren, L., Guo, L., Guo, R., Chen, T., Hu, J.*, et al.* (2020). Characterization of spike glycoprotein of SARS-CoV-2 on virus entry and its immune cross-reactivity with SARS-CoV. Nat Commun *11*, 1620.

Papa, G., Mallery, D.L., Albecka, A., Welch, L.G., Cattin-Ortolá, J., Luptak, J., Paul, D., McMahon, H.T., Goodfellow, I.G., Carter, A.*, et al.* (2021). Furin cleavage of SARS-CoV-2 Spike promotes but is not essential for infection and cell-cell fusion. PLoS Pathog *17*, e1009246.

Peacock, T.P., Brown, J.C., Zhou, J., Thakur, N., Newman, J., Kugathasan, R., Sukhova, K., Kaforou, M., Bailey, D., and Barclay, W.S. (2022). The SARS-CoV-2 variant, Omicron, shows rapid replication in human primary nasal epithelial cultures and efficiently uses the endosomal route of entry. bioRxiv, 2021.2012.2031.474653.

Peacock, T.P., Goldhill, D.H., Zhou, J., Baillon, L., Frise, R., Swann, O.C., Kugathasan, R., Penn, R., Brown, J.C., Sanchez-David, R.Y.*, et al.* (2021a). The furin cleavage site in the SARS-CoV-2 spike protein is required for transmission in ferrets. Nat Micro *6*, 899-909.

Peacock, T.P., Sheppard, C.M., Brown, J.C., Goonawardane, N., Zhou, J., Whiteley, M., Consortium, P.V., de Silva, T.I., and Barclay, W.S. (2021b). The SARS-CoV-2 variants

associated with infections in India, B.1.617, show enhanced spike cleavage by furin. bioRxiv, 2021.2005.2028.446163.

Petrillo, C., Thorne, L.G., Unali, G., Schiroli, G., Giordano, A.M.S., Piras, F., Cuccovillo, I., Petit, S.J., Ahsan, F., Noursadeghi, M.*, et al.* (2018). Cyclosporine H Overcomes Innate Immune Restrictions to Improve Lentiviral Transduction and Gene Editing In Human Hematopoietic Stem Cells. Cell Stem Cell *23*, 820-832.e829.

Pizzato, M., Erlwein, O., Bonsall, D., Kaye, S., Muir, D., and McClure, M.O. (2009). A one-step SYBR Green I-based product-enhanced reverse transcriptase assay for the quantitation of retroviruses in cell culture supernatants. J Virol Methods *156*, 1-7.

Plante, J.A., Liu, Y., Liu, J., Xia, H., Johnson, B.A., Lokugamage, K.G., Zhang, X., Muruato, A.E., Zou, J., Fontes-Garfias, C.R.*, et al.* (2021). Spike mutation D614G alters SARS-CoV-2 fitness. Nature *592*, 116-121.

Prelli Bozzo, C., Nchioua, R., Volcic, M., Koepke, L., Krüger, J., Schütz, D., Heller, S., Stürzel, C.M., Kmiec, D., Conzelmann, C.*, et al.* (2021). IFITM proteins promote SARS-CoV-2 infection and are targets for virus inhibition in vitro. Nat Commun *12*, 4584.

Rajah, M.M., Hubert, M., Bishop, E., Saunders, N., Robinot, R., Grzelak, L., Planas, D., Dufloo, J., Gellenoncourt, S., Bongers, A.*, et al.* (2021). SARS-CoV-2 Alpha, Beta, and Delta variants display enhanced Spike-mediated syncytia formation. EMBO J *40*, e108944.

Rees-Spear, C., Muir, L., Griffith, S.A., Heaney, J., Aldon, Y., Snitselaar, J.L., Thomas, P., Graham, C., Seow, J., Lee, N.*, et al.* (2021). The effect of spike mutations on SARS-CoV-2 neutralization. Cell Rep *34*, 108890.

Rogers, T.F., Zhao, F., Huang, D., Beutler, N., Burns, A., He, W.T., Limbo, O., Smith, C., Song, G., Woehl, J.*, et al.* (2020). Isolation of potent SARS-CoV-2 neutralizing antibodies and protection from disease in a small animal model. Science *369*, 956-963.

Saito, A., Irie, T., Suzuki, R., Maemura, T., Nasser, H., Uriu, K., Kosugi, Y., Shirakawa, K., Sadamasu, K., Kimura, I.*, et al.* (2022). Enhanced fusogenicity and pathogenicity of SARS-CoV-2 Delta P681R mutation. Nature *602*, 300-306.

Schindelin, J., Arganda-Carreras, I., Frise, E., Kaynig, V., Longair, M., Pietzsch, T., Preibisch, S., Rueden, C., Saalfeld, S., Schmid, B.*, et al.* (2012). Fiji: an open-source platform for biological-image analysis. Nat Methods *9*, 676-682.

Schmidt, F., Weisblum, Y., Muecksch, F., Hoffmann, H.H., Michailidis, E., Lorenzi, J.C.C., Mendoza, P., Rutkowska, M., Bednarski, E., Gaebler, C.*, et al.* (2020). Measuring SARS-CoV-2 neutralizing antibody activity using pseudotyped and chimeric viruses. J Exp Med *217*.

Seow, J., Graham, C., Merrick, B., Acors, S., Pickering, S., Steel, K.J.A., Hemmings, O., O'Byrne, A., Kouphou, N., Galao, R.P.*, et al.* (2020). Longitudinal observation and decline of neutralizing antibody responses in the three months following SARS-CoV-2 infection in humans. Nat Microbiol *5*, 1598-1607.

Shi, G., Kenney, A.D., Kudryashova, E., Zani, A., Zhang, L., Lai, K.K., Hall-Stoodley, L., Robinson, R.T., Kudryashov, D.S., Compton, A.A.*, et al.* (2021). Opposing activities of IFITM proteins in SARS-CoV-2 infection. EMBO J *40*, e106501.

Shuai, H., Chan, J.F.-W., Hu, B., Chai, Y., Yuen, T.T.-T., Yin, F., Huang, X., Yoon, C., Hu, J.-C., Liu, H.*, et al.* (2022). Attenuated replication and pathogenicity of SARS-CoV-2 B.1.1.529 Omicron. Nature. Online ahead of print DOI: 10.1038/s41586-022-04442-5

Temmam, S., Vongphayloth, K., Salazar, E.B., Munier, S., Bonomi, M., Regnault, B., Douangboubpha, B., Karami, Y., Chrétien, D., Sanamxay, D.*, et al.* (2022). Bat coronaviruses related to SARS-CoV-2 and infectious for human cells. Nature. Online ahead of print DOI: 10.1038/s41586-022-04442-5

Thorne, L.G., Bouhaddou, M., Reuschl, A.K., Zuliani-Alvarez, L., Polacco, B., Pelin, A., Batra, J., Whelan, M.V.X., Hosmillo, M., Fossati, A.*, et al.* (2022). Evolution of enhanced innate immune evasion by SARS-CoV-2. Nature *602*, 487-495.

Thorne, L.G., Reuschl, A.K., Zuliani-Alvarez, L., Whelan, M.V.X., Turner, J., Noursadeghi, M., Jolly, C., and Towers, G.J. (2021). SARS-CoV-2 sensing by RIG-I and MDA5 links epithelial infection to macrophage inflammation. EMBO J *40*, e107826.

Walls, A.C., Park, Y.J., Tortorici, M.A., Wall, A., McGuire, A.T., and Veesler, D. (2020). Structure, Function, and Antigenicity of the SARS-CoV-2 Spike Glycoprotein. Cell *181*, 281-292 e286.

Willett, B.J., Grove, J., MacLean, O.A., Wilkie, C., Logan, N., Lorenzo, G.D., Furnon, W., Scott, S., Manali, M., Szemiel, A.*, et al.* (2022). The hyper-transmissible SARS-CoV-2 Omicron variant exhibits significant antigenic change, vaccine escape and a switch in cell entry mechanism. medRxiv, 2022.2001.2003.21268111.

Winstone, H., Lista, M.J., Reid, A.C., Bouton, C., Pickering, S., Galao, R.P., Kerridge, C., Doores, K.J., Swanson, C.M., and Neil, S.J.D. (2021). The Polybasic Cleavage Site in SARS-CoV-2 Spike Modulates Viral Sensitivity to Type I Interferon and IFITM2. J Virol *95*. e02422-20.

Xia, S., Zhu, Y., Liu, M., Lan, Q., Xu, W., Wu, Y., Ying, T., Liu, S., Shi, Z., Jiang, S.*, et al.* (2020). Fusion mechanism of 2019-nCoV and fusion inhibitors targeting HR1 domain in spike protein. Cell Mol Immunol *17*, 765-767.

Yurkovetskiy, L., Wang, X., Pascal, K.E., Tomkins-Tinch, C., Nyalile, T.P., Wang, Y., Baum, A., Diehl, W.E., Dauphin, A., Carbone, C.*, et al.* (2020). Structural and Functional Analysis of the D614G SARS-CoV-2 Spike Protein Variant. Cell *183*, 739-751.e738.

Ziegler, C.G.K., Allon, S.J., Nyquist, S.K., Mbano, I.M., Miao, V.N., Tzouanas, C.N., Cao, Y., Yousif, A.S., Bals, J., Hauser, B.M.*, et al.* (2020). SARS-CoV-2 Receptor ACE2 Is an Interferon-Stimulated Gene in Human Airway Epithelial Cells and Is Detected in Specific Cell Subsets across Tissues. Cell *181*, 1016-1035.e1019.

## Figure legends

### Figure 1: GBP2 and 5 inhibit Wuhan-Hu-1 and Omicron, but not Alpha and Delta spike-mediated infectivity

**A)** Schematic of SARS-CoV-2 spike subunit and main domain boundaries, with positions of S1/S2 and S2' cleavage sites and linage defining mutations in the VOCs are indicated. NTD, N-terminal domain; RBD, receptor-binding domain; FP, fusion peptide; HR, heptad repeat.
**B)** Expression of HA-tagged GBPs in PV-producing 293T cells as measured by flow

cytometry. **C-G)** Infectivity of PVs produced by 293T cells made in the presence of increasing amounts of plasmid encoding GBP2, GBP2 C588A, GBP5, GBP5 C583A or empty vector control was measured by luciferase assay (RLU) on Caco2 cells. Data show the percentage infectivity of PV made in the presence of GBPs normalised to empty vector control (no GBP, set to 100%). Percent infectivity of **C)** Wuhan-Hu-1, **D)** Wuhan-Hu-1 D614G, **E)** Alpha, **F)** Delta, and **G)** Omicron spike PV infection are shown. **H)** Comparison of particle infectivity (RLU/RT) of spike PVs on Caco2 cells made in the absence of GBPs. Data show the mean ±SEM from three independent experiments**. C-G)** Statistical analysis was performed by two-way ANOVA with Dunnett's multiple comparisons test. **H)** One-way ANOVA with Dunnett's multiple comparisons test. Asterisks for p values denote statistical significance for GBPs (120 ng) compared EV control. Ns, not significant; *P < 0.05; **P < 0.01; ***P < 0.001; ****P < 0.0001.

**Figure 2: GBP2 and 5 inhibit SARS-CoV-2 spike cleavage**

Spike PVs were produced in 293T cells in the presence of 80 ng of GBP plasmid or empty vector (EV) control. PV purified from culture supernatants and cell lysates were immunoblotted for spike, lentiviral Gag (p24 and p55), GBP (HA-tag) and tubulin. **A)** Immunoblot of Wuhan-Hu-1 PV spike produced by 293T cells made in presence of GBP2/5 and their mutants or EV control. **B)** Corresponding 293T cell lysate from A. **C)** Immunoblot of VOC spike PV produced in presence of GBP5 or EV and **D)** the corresponding cell lysates. Representative immunoblots are shown. Graphs show band densitometry quantification pooled from three independent experiments, measuring the relative proportion of cleaved spike in PV and cell lysates (S2/S), cleaved spike incorporation into PV (S2/p24) and total spike incorporation (S2+S)/p24). Bars show mean and individual values. Statistical analysis was performed using a two-tailed paired t test. Ns, not significant; *P < 0.05; **P < 0.01; ***P < 0.001; ****P < 0.0001.

**Figure 3: Effects of GBPs on spike-mediated entry pathways in Caco2 cells**

Inhibition of spike-mediated PV infection of Caco2 cells by **A)** Camostat and **B)** E64d inhibitors. Shown is a representative titration. **C)** Inhibition of spike PV infection Caco2 cells in the presence of 25 μM Camostat or 25 μM E64d normalised to DMSO control. Infection was measured by luciferase assay. **D)** Inhibition of SARS-CoV-2 live virus infection of Caco2 cells in presence of 25 μM Camostat or 25 μM E64d. Infection was measured by flow cytometry staining for nucleoprotein and shown as the percentage N-positive cells (% N+). Left panel shows percentage N+ cells at 24 hpi, and the right panel shows the percentage infection for each virus normalised to the corresponding DMSO control. **E)** Immunoblot analysis of spike cleavage in SARS-CoV-2 virions. Indicated virus isolates were purified from

culture supernatants and immunoblotted for spike and nucleoprotein. Band quantification shows relative proportion of cleaved spike (S2/S) and cleaved spike incorporation into virions (S2/N). **F-H)** Effect of GBPs on SARS-CoV-2 spike-mediated entry pathways. Wuhan-Hu-1 spike PV made in presence of 80 ng of indicated GBP plasmid or EV control was used to infect Caco2 cells in the presence of increasing concentrations of **F)** Camostat or **G)** E64d. Data show percentage infection compared to DMSO EV control. **H)** Inhibition of Wuhan-Hu-1 PV +/-GBPs and in the presence of 25 μM Camostat or 25 μM E64d. Data are normalised to DMSO control separately for each GBP treatment and grouped by inhibitor treatment. **I-J)** Omicron spike PV was made in presence of GBP5 or EV control and infection of Caco2 cells in the presence of increasing doses of **(I)** Camostat or **(J)** E64d. Data show the mean ±SEM from three independent experiments. Groups were compared using a two-way ANOVA with Dunnett's multiple comparisons test. Ns, not significant; *P < 0.05; **P < 0.01; ***P < 0.001; ****P < 0.0001.

**Figure 4: IFITM restriction of SARS-CoV-2 and the interplay with GBPs**

**A)** Expression of HA-tagged IFITMs in Caco2 cells stably expressing IFITM1-3 as measured by flow cytometry. Left panel shows a representative histogram. **B)** Immunofluorescence images of stable Caco2 cells expressing IFITM1-3. HA-tag IFITM shown in green, CD63 shown in red, and nuclei shown in blue. Scale bar is 50 μm. **C-G)** Caco2 cells expressing IFITMs were infected with live SARS-CoV-2 virus. Shown is percent N+ cells after 24 hpi of **C)** VIC, **D)** IC19, **E)** Alpha, **F)** Delta, and **G)** Omicron isolates. **H-L)** PV infection of IFITM transduced Caco2 cells with **H)** Wuhan-Hu-1, **I)** Wuhan-Hu-1 D614G, **J)** Alpha, **K)** Delta, and **L)** Omicron spike PV. Data are shown as percent infectivity normalised to WT Caco2 cells (no IFITM over-expression). **M)** Caco2 cells expressing IFITMs were incubated with Camostat inhibitor (5 μM) or DMSO control and infected with Wuhan-Hu-1 PV. Percent infectivity was determined by normalising to WT Caco2 cells DMSO control. **N-R)** IFITM expressing Caco2 cells were infected with spike PVs made in presence of GBP5 or EV control. Data show the infectivity normalised to EV control on WT cells for PV made using **N)** Wuhan-Hu-1, **O)** Wuhan-Hu-1 D614G, **P)** Alpha, **Q)** Delta, and **R)** Omicron spikes. Data show the mean ±SEM from three independent experiments. Groups were compared **A-L)** using a one-way ANOVA or **M-R)** using a two-way ANOVA with Dunnett's multiple comparisons test. Ns, not significant; *P < 0.05; **P < 0.01; ***P < 0.001; ****P < 0.0001.

**Figure 5: Omicron spike C-terminal truncation increases PV infectivity, but does not rescue from GBP or IFITM restriction**

Omicron spike PV were produced in presence of GBP5 or EV control using plasmids encoding either full-length (FL) or a 19 residue C-terminal truncation (ΔCT) Omicron spike

sequence. Spike PV were titrated on WT Caco2 cells, showing **A)** raw infectivity (RLU/RT) values in absence of GBP5 expression (EV control) and **B)** percent infectivity normalised to EV control for each Omicron spike (FL and ΔCT). **C-F)** Indicated Omicron PV were titrated on Caco2 WT and IFITM expressing cells. Shown is infectivity normalised to EV control for **C)** FL Omicron PV, **D)** ΔCT Omicron PV, **E)** FL Omicron PV made in presence of GBP5 or EV control and **F)** ΔCT Omicron PV made in presence of GBP5 or EV control. Bars show mean ±SEM from three independent experiments. Groups were compared **A-B)** using a two-tailed paired t test, **C-D)** using a one-way ANOVA or **E-F)** using a two-way ANOVA with Dunnett's multiple comparisons test. Ns, not significant; *P < 0.05; **P < 0.01; ***P < 0.001; ****P < 0.0001.

**Supplementary Figure 1: GBP restriction of HIV-1 Env, SARS-CoV-2, SARS-CoV-1 and MERS-CoV spike-mediated infection**

**A)** Schematic of the pseudovirus (PV) infection assay. 293T cells were co-transfected with lentiviral packaging, luciferase reporter and spike plasmids (to make PV) and GBP vector or empty vector (EV) control. PV-containing supernatant was used to infect indicated cells lines and infection was quantified by measuring luciferase expression by luminometry. PV content in the supernatants was measured by SG-PERT qPCR assay. Created with BioRender.com **B)** HIV Env (JRFL) PV or **C)** HIV-1 live virus (NL4.3) were produced in 293T cells in presence of increasing amounts of plasmid encoding GBP2, GBP2 C588A, GBP5, GBP5 C583A or empty vector control and infection was measured by luciferase assay (RLU) on HeLa-TZMbl reporter cell line. Data show the percentage infectivity of PV made in the presence of GBPs normalised to empty vector control (no GBP, set to 100%). **D)** Expression of HA-tagged GBP2 in PV-producing 293T cells as measured by flow cytometry. Shown is a representative histogram, related to Fig. 1B. **E-I)** Spike PV were produced in presence of increasing doses of GBP2/5, GBP mutants or EV control and infection was measured on indicated cell lines (as described in A). Shown is percent infectivity normalised to EV control for **E)** SARS-CoV-2 Wuhan-Hu-1 spike PV titrated on Vero.E6 cells, **F)** MERS-CoV spike PV titrated on Caco2 cells, and SARS-CoV-1 spike PV titrated on **G)** Caco2, **H)** HeLA-ACE2, and **I)** Vero.E6 cells. **J-O)** SARS-CoV-2 spike PV made in presence of increasing doses of GBP2/5 or their mutants were titrated on HeLa-ACE2 cells (as described above). Shown is percent infectivity normalised to EV control for **J)** Wuhan-Hu-1, **K)** Wuhan-Hu-1 D614G, **L)** Alpha, **M)** Delta, and **N)** Omicron spike PV infection. **O)** Comparison of particle infectivity (RLU/RT) of spike PVs on HeLa-ACE2 cells made in the absence of GBPs. Shown is mean ±SEM from three independent experiments**. A-N)** Two-way ANOVA with Dunnett's multiple comparisons test. Asterisks for p values denote statistical significance for GBPs (120 ng)

compared EV control. **O)** RM one-way ANOVA with Dunnett's multiple comparisons test. Ns, not significant; *P < 0.05; **P < 0.01; ***P < 0.001; ****P < 0.0001.

**Supplementary Figure 2: GBPs do not impact SARS-CoV-2 Spike cell surface expression**

293T cells were transfected with Wuhan-Hu-1 spike, lentiviral packaging and reporter plasmids and increasing doses of GBP2/5 or GBP mutants. Cells were harvested, stained for cell surface expression of spike and intracellular expression of HA-tagged GBPs. **A)** Shown are representative histograms of spike expression in HA+ live cell population. **B)** Cell surface expression of spike (MFI) in the Spike+HA+ live cell population. Shown is mean ±SEM from three independent experiments. Different GBP treatments were compared to EV control using a RM one-way ANOVA with Dunnett's multiple comparisons test. Ns, not significant, P > 0.05.

**Supplementary Figure 3: Lower expression of spike restores GBP restriction**

Spike PVs were produced with fixed amount of GBP2/5 vector or EV control (80 ng) and decreasing doses of spike plasmid (40 ng being the amount used elsewhere in this study). Upper panels show raw infectivity values (RLU/RT) and lower panels show percent infectivity of GBP2/5 PVs normalised to EV control at each dose of spike plasmid. **A)** Wuhan-Hu-1, **B)** Wuhan-Hu-1 D614G, **C)** Alpha, **D)** Delta, and **E)** Omicron spike PV titrated on Caco2 cells. **F)** Wuhan-Hu-1, **G)** Wuhan-Hu-1 D614G, **H)** Alpha, **I)** Delta, and **J)** Omicron spike PV titrated on HeLa-ACE2 cells. Shown is mean ±SEM from three independent experiments. Groups were compared using a two-way ANOVA with Dunnett's multiple comparisons test. Asterisks for p values denote statistical significance for GBP2/5 treatment compared EV control. Ns, not significant; *P < 0.05; **P < 0.01; ***P < 0.001; ****P < 0.0001.

**Supplementary Figure 4: SARS-CoV-2 favours endosomal entry in HeLa-ACE2 cells**

Inhibition of spike-mediated PV infection of HeLa-ACE2 cells by **A)** Camostat and **B)** E64d inhibitors. Shown is a representative titration. **C)** Inhibition of spike PV infection of HeLa-ACE2 cells in the presence of 25 μM Camostat or 25 μM E64d normalised to DMSO control. Infection was measured by luciferase assay. **D)** Inhibition of SARS-CoV-2 live virus infection of HeLa-ACE2 cells in presence of 25 μM Camostat or 25 μM E64d. Infection was measured by flow cytometry staining for nucleoprotein and shown as the percentage N-positive cells (% N+). Left panel shows percentage N+ cells at 24 hpi, and the right panel shows the percentage infection for each virus normalised to the corresponding DMSO control. Shown is mean ±SEM from three independent experiments. Groups were compared using a two-

way ANOVA with Dunnett's multiple comparisons test. Ns, not significant; *P < 0.05; **P < 0.01; ***P < 0.001; ****P < 0.0001.

**Supplementary Figure 5: PV Infection and GBP5 inhibition across cell lines**
Indicated spike PV were made in presence of 80 ng GBP5 or EV control and used to infect indicated cell lines: Caco2, HeLa-ACE2, 293T-ACE2, Vero.E6-TMPRSS2 and Vero.E6 WT. **A)** Shown are raw infectivity (RLU/RT) values for infection with PV made in absence of GBP5 (EV control). **B)** Shown is percent infectivity of PV made in presence of GBP5 normalised to EV control for each spike PV titrated on each cell line. Shown is mean ±SEM from three independent experiments.

# Figure 1

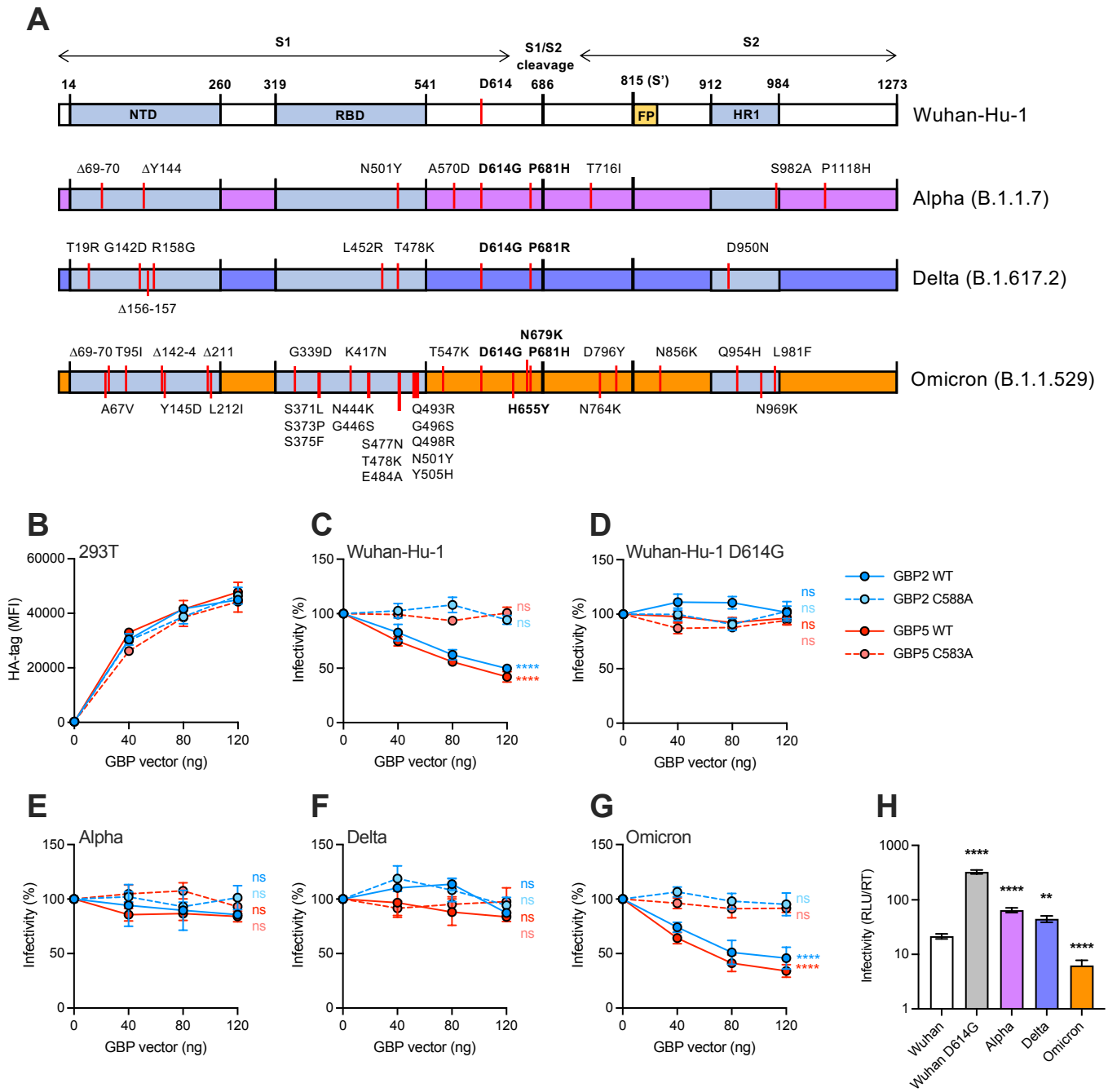
A
S1
S1/S2 cleavage
S2
14
260
319
541
D614
686
815 (S')
912
984
1273
NTD
RBD
FP
HR1
Wuhan-Hu-1
Δ69-70 ΔY144 N501Y A570D D614G P681H T716I S982A P1118H
Alpha (B.1.1.7)
T19R G142D R158G L452R T478K D614G P681R D950N
Δ156-157
Delta (B.1.617.2)
N679K
Δ69-70 T95I Δ142-4 Δ211 G339D K417N T547K D614G P681H D796Y N856K Q954H L981F
A67V Y145D L212I S371L S373P S375F N444K G446S S477N T478K E484A Q493R Q496S Q498R N501Y Y505H H655Y N764K N969K
Omicron (B.1.1.529)
B
293T
HA-tag (MFI)
GBP vector (ng)
C
Wuhan-Hu-1
Infectivity (%)
D
Wuhan-Hu-1 D614G
GBP2 WT
GBP2 C588A
GBP5 WT
GBP5 C583A
E
Alpha
F
Delta
G
Omicron
H
Infectivity (RLU/RT)
Wuhan
Wuhan D614G
Alpha
Delta
Omicron

# Figure 2

Wuhan-Hu-1

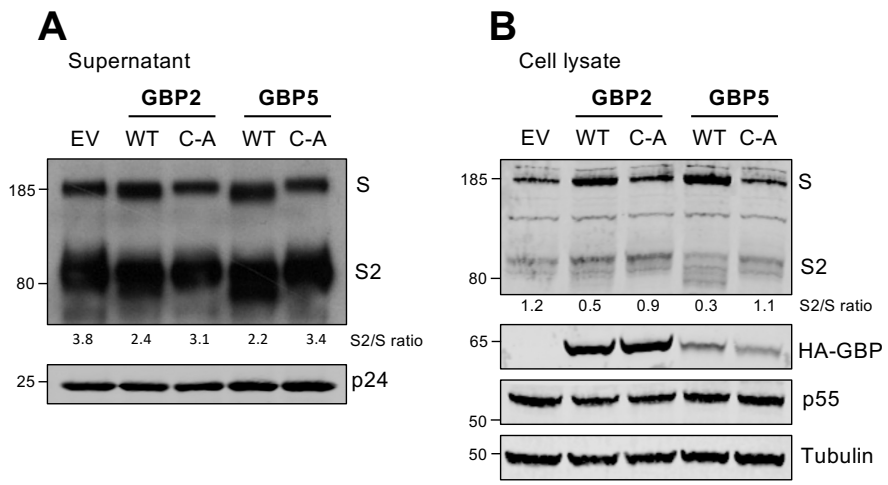


VOCs

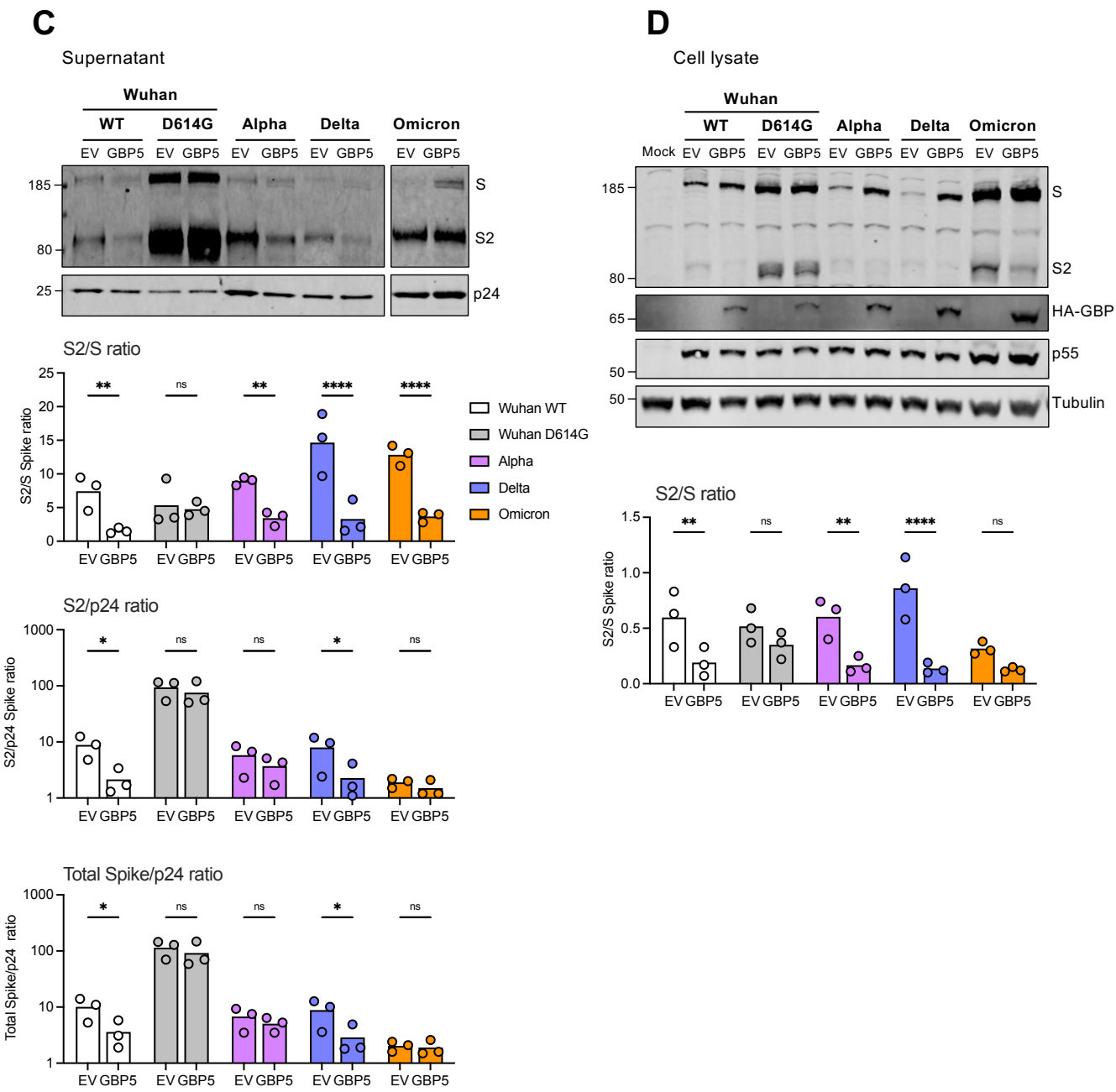

# Figure 3

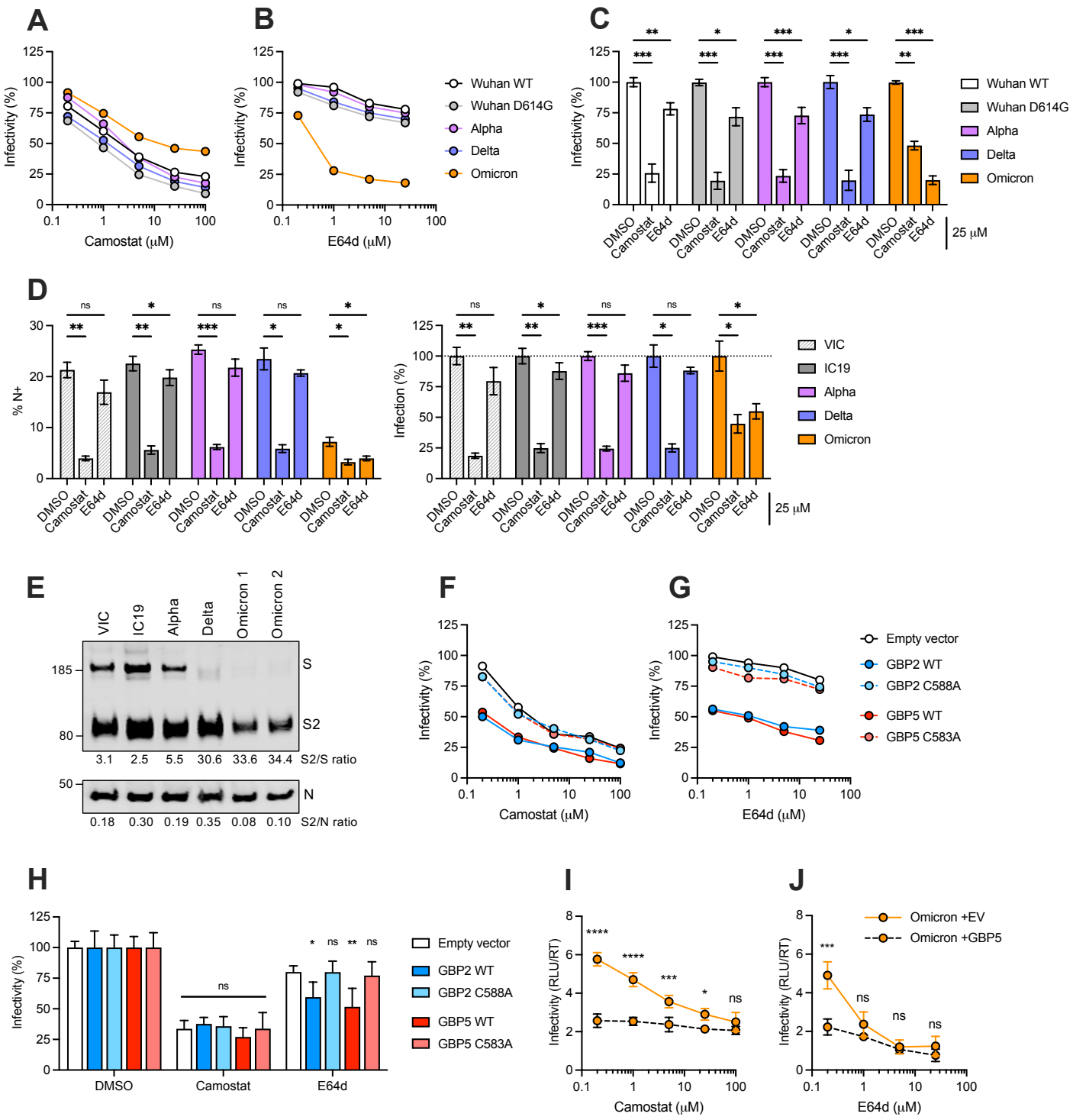
A
Infectivity (%)
Camostat (μM)
B
E64d (μM)
Wuhan WT
Wuhan D614G
Alpha
Delta
Omicron
C
DMSO
Camostat
E64d
25 μM
D
% N+
Infection (%)
VIC
IC19
E
S
S2
N
S2/S ratio
S2/N ratio
F
G
Empty vector
GBP2 WT
GBP2 C588A
GBP5 WT
GBP5 C583A
H
I
J
Infectivity (RLU/RT)
Omicron +EV
Omicron +GBP5

# Figure 4

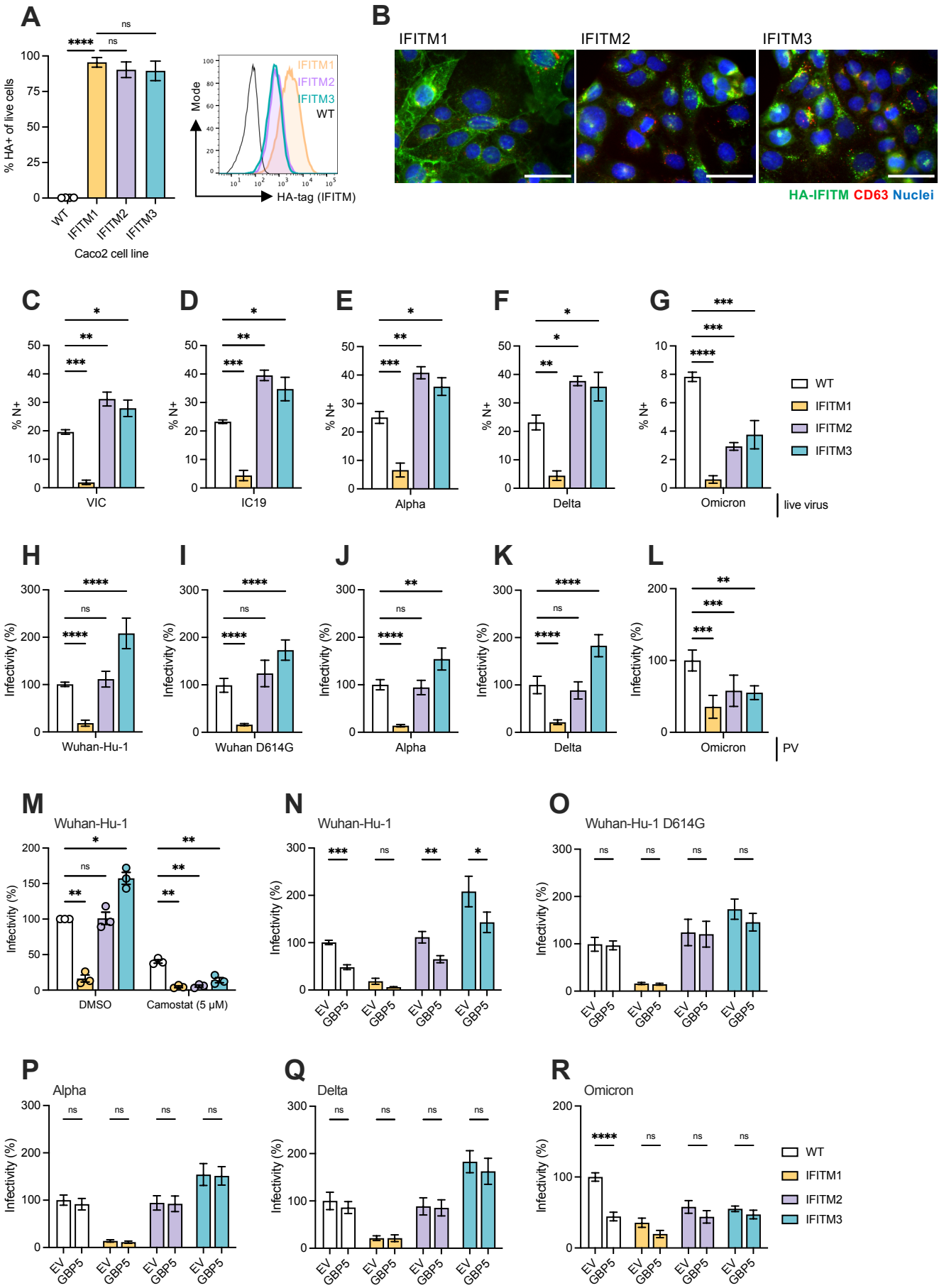
A
% HA+ of live cells
WT
IFITM1
IFITM2
IFITM3
Caco2 cell line
Mode
HA-tag (IFITM)
B
IFITM1
IFITM2
IFITM3
HA-IFITM CD63 Nuclei
C
D
E
F
G
% N+
VIC
IC19
Alpha
Delta
Omicron
live virus
H
I
J
K
L
Infectivity (%)
Wuhan-Hu-1
Wuhan D614G
PV
M
N
O
Wuhan-Hu-1
Wuhan-Hu-1 D614G
DMSO
Camostat (5 μM)
EV
GBP5
P
Q
R
Alpha
Delta
Omicron

# Figure 5

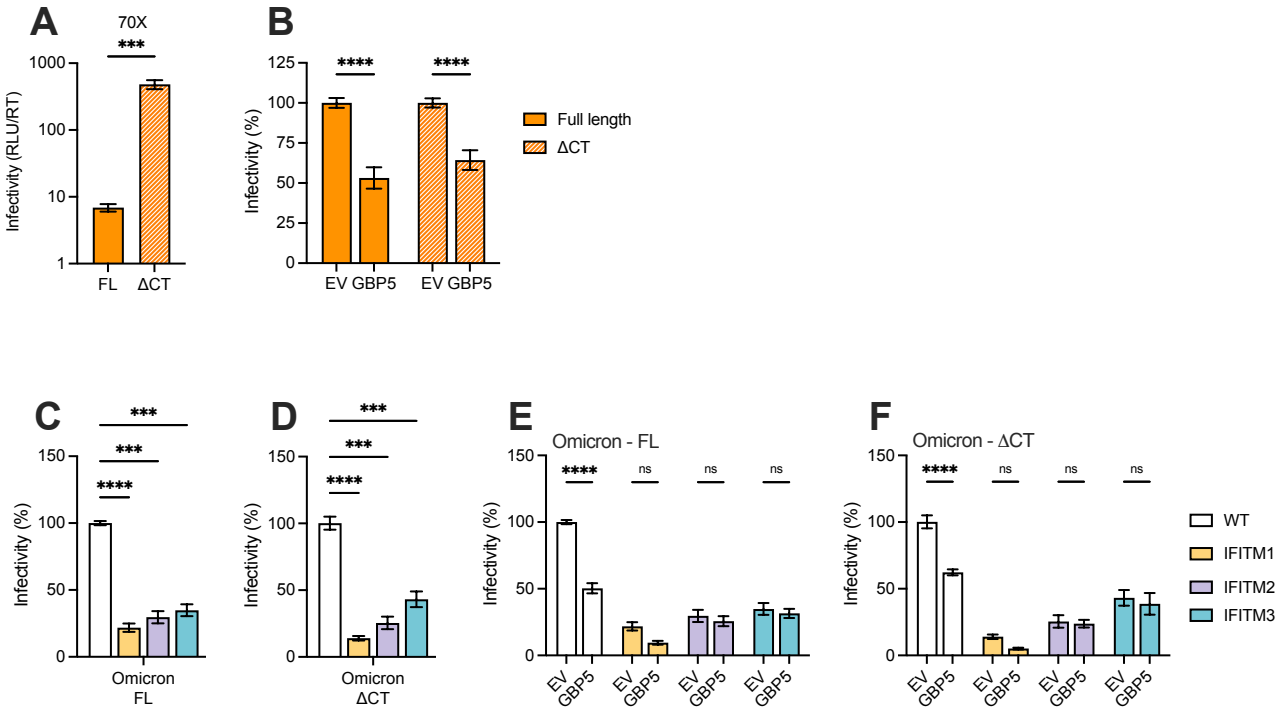
A
70X
***
Infectivity (RLU/RT)
1000
100
10
1
FL
ΔCT
B
****
****
Infectivity (%)
125
100
75
50
25
0
EV GBP5
EV GBP5
Full length
ΔCT
C
***
***
****
Infectivity (%)
150
100
50
0
Omicron FL
D
***
***
****
Infectivity (%)
150
100
50
0
Omicron ΔCT
E
Omicron - FL
****
ns
ns
ns
Infectivity (%)
150
100
50
0
EV GBP5
EV GBP5
EV GBP5
EV GBP5
F
Omicron - ΔCT
****
ns
ns
ns
Infectivity (%)
150
100
50
0
EV GBP5
EV GBP5
EV GBP5
EV GBP5
WT
IFITM1
IFITM2
IFITM3

## Supplementary figure 1

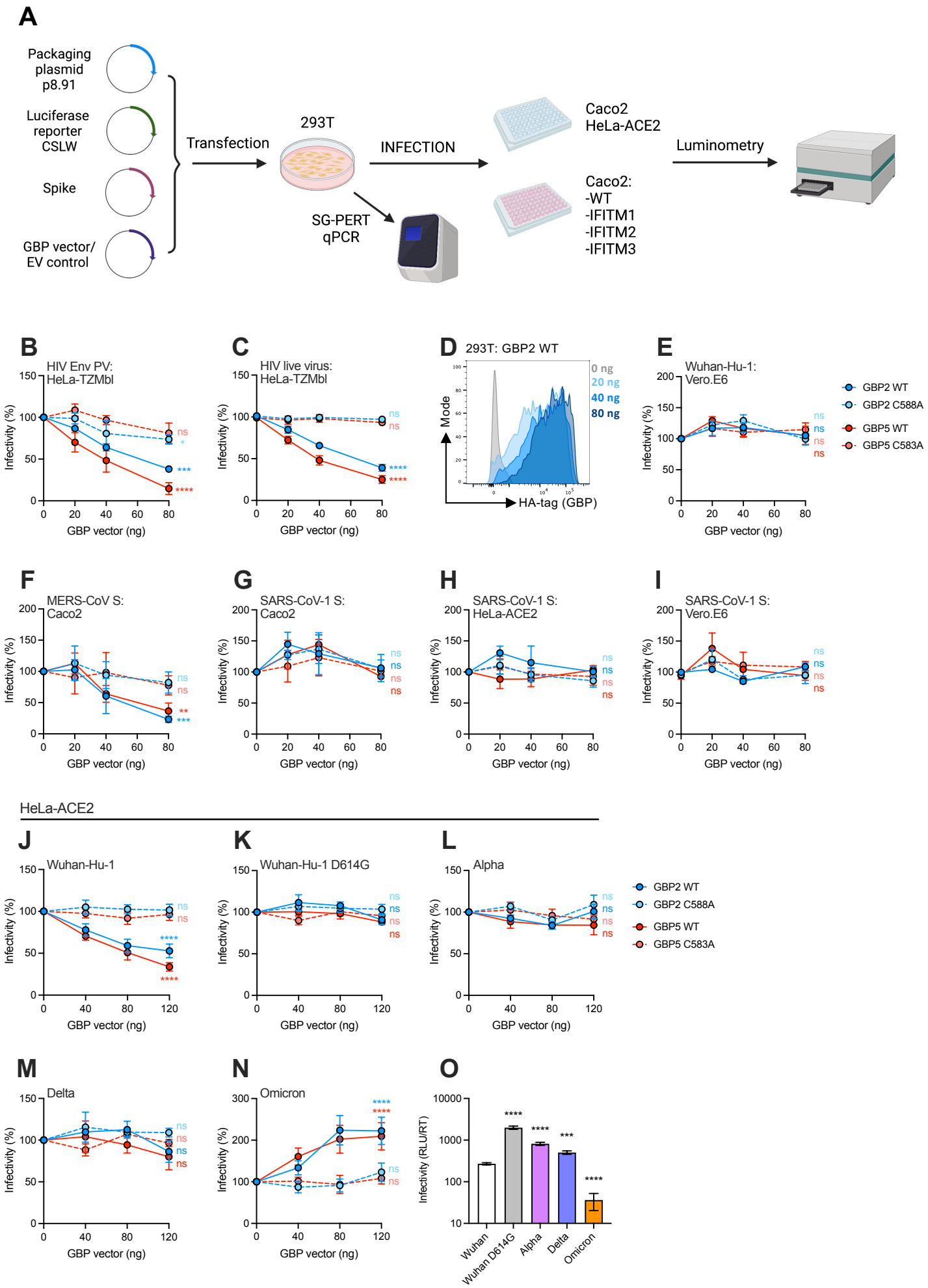

## Supplementary figure 2

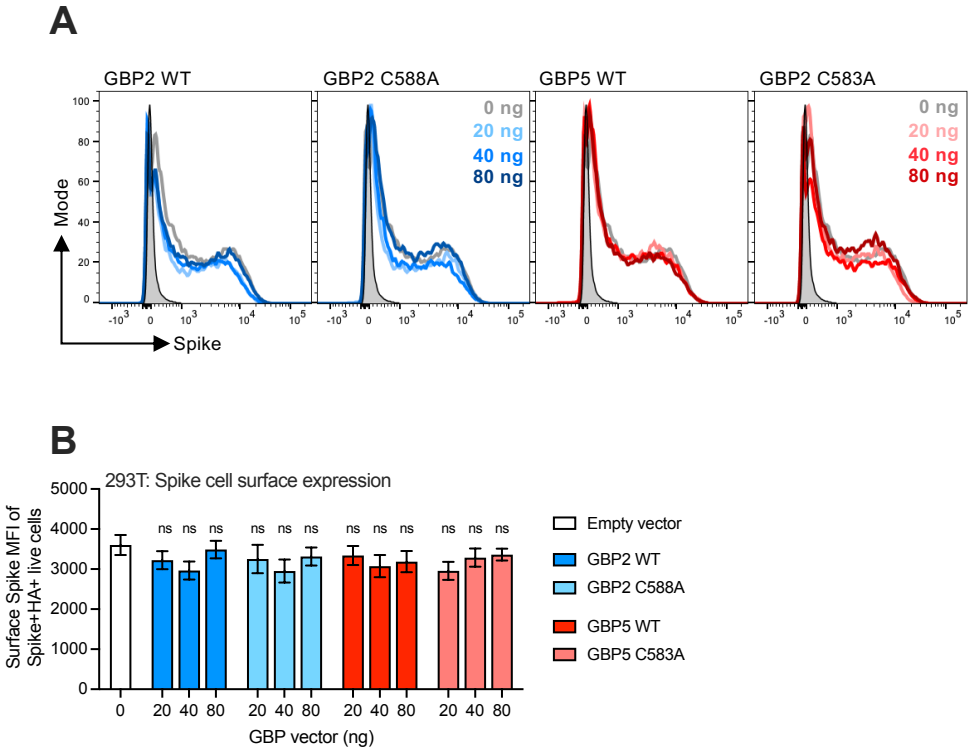

# Supplementary figure 3

Caco2

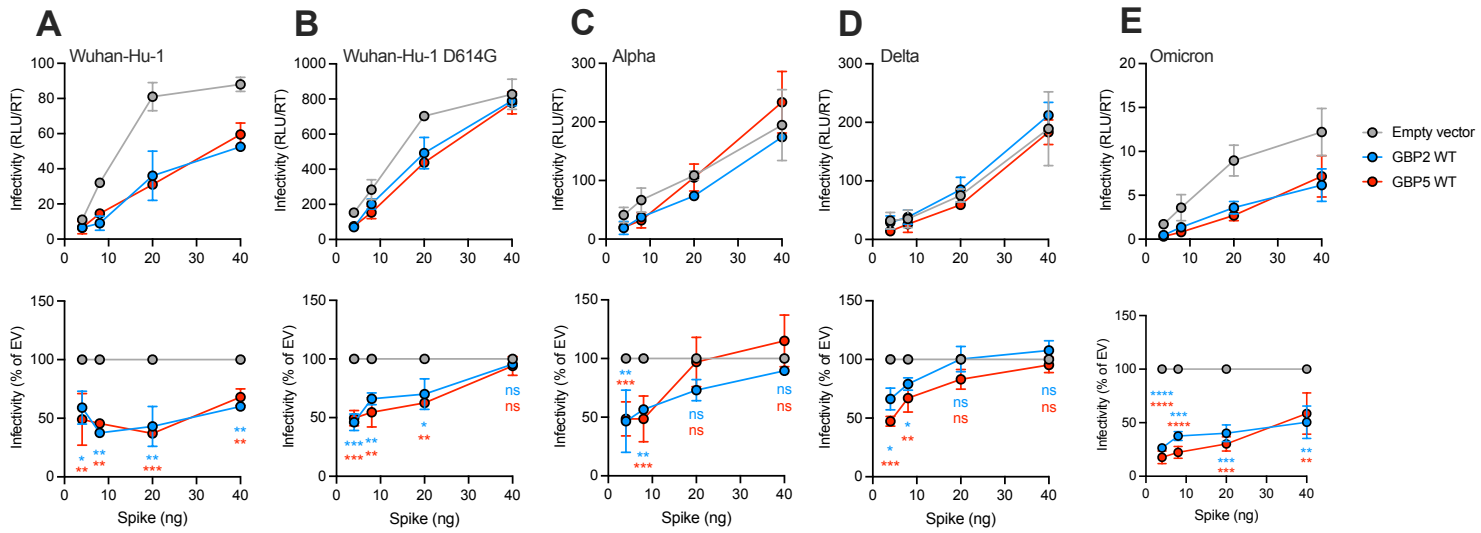


HeLa-ACE2

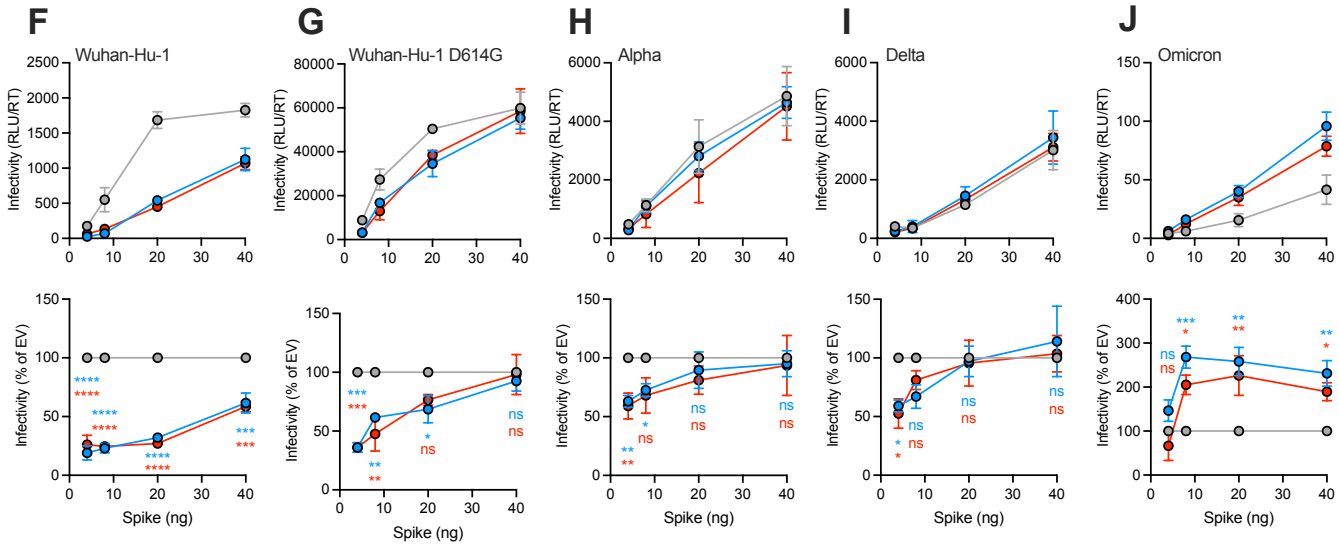

## Supplementary figure 4

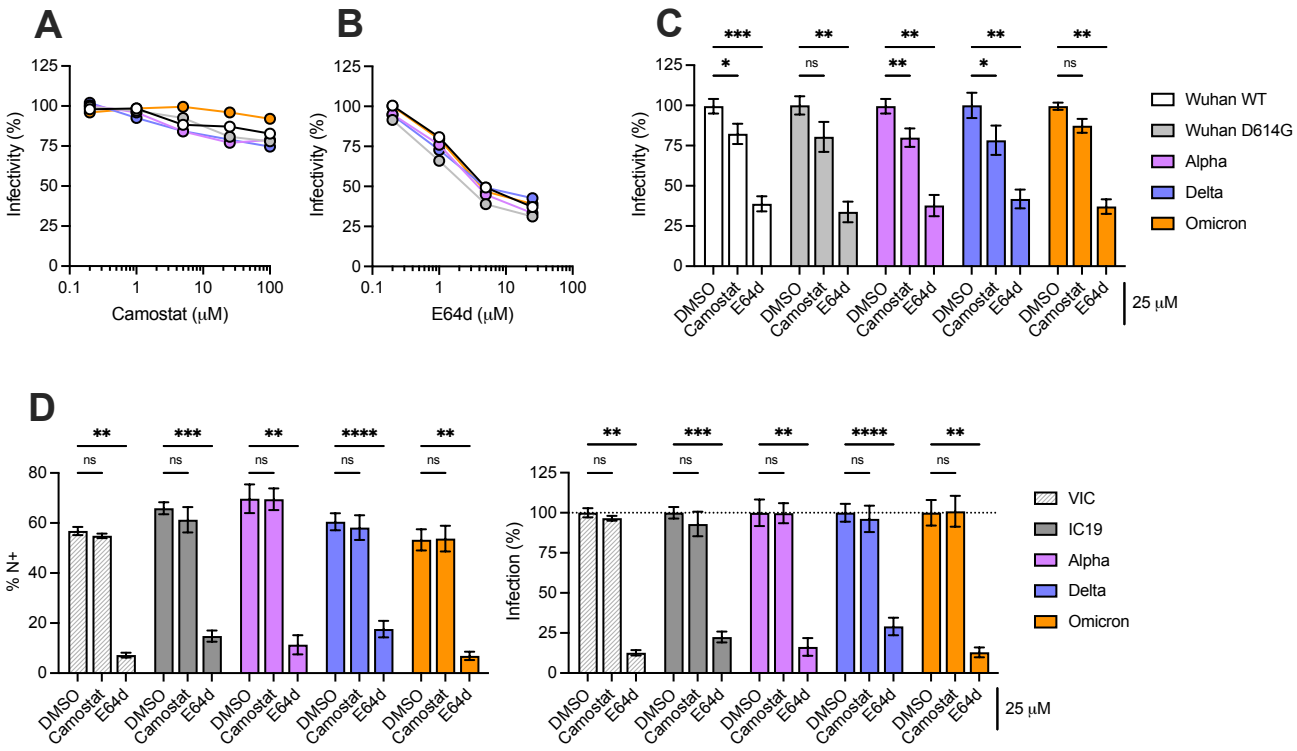
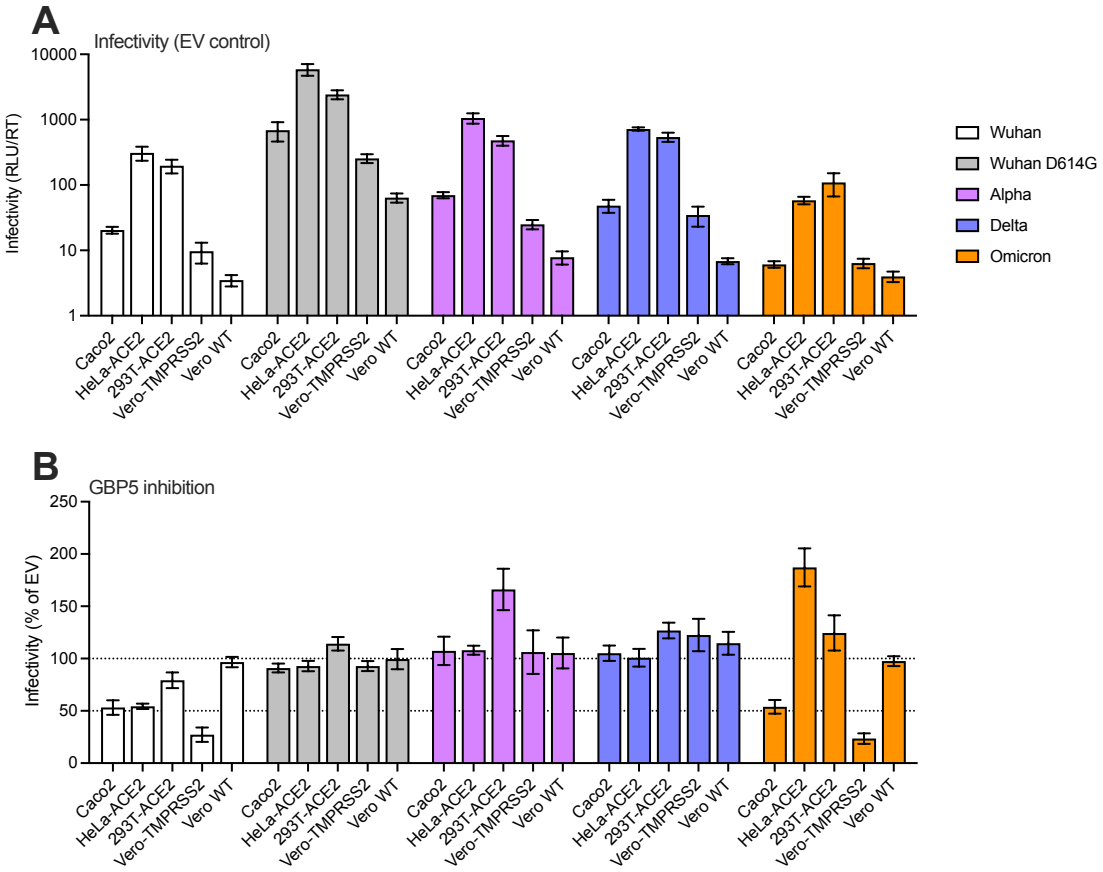
## Supplementary figure 5